Formation of Double Compact Objects

V. Kalogera [a], K. Belczynski [b], C. Kim [c], R. O'Shaughnessy [a], & B. Willems [a]

[a] *Department of Physics & Astronomy, Northwestern University, 2145 Sheridan Rd, Evanston, IL 60208*

[b] *Department of Astronomy, New Mexico State University, 1320 Frenger Mall, Las Cruces, NM 88003*

[c] *Department of Astronomy, Cornell University, 522 Space Sicences Building, Ithaca, NY 14853*

Abstract

Current observations of double neutron stars provide us with a wealth of information that we can use to investigate their evolutionary history and the physical conditions of neutron star formation. Understanding this history and formation conditions further allow us to make theoretical predictions for the formation of other double compact objects with one or two black hole components and assess the detectability of such systems by ground-based gravitational-wave interferometers. In this paper we summarize our group's body of work in the past few years and we place our conclusions and current understanding in the framework of other work in this area of astrophysical research.

Key words: neutron stars, black holes, pulsars, binaries, supernovae, gravitational waves

1 Introduction

Gravitational waves were theoretically predicted many decades ago by Einstein and his theory of General Relativity, and their existence has been indirectly confirmed by the pioneering observations of the Hulse-Taylor binary pulsar (Hulse & Taylor 1975). In the coming years, the physics and astronomy community anticipates the first direct detection of gravitational waves (GW) and the birth of a new research field: GW astrophysics, where observations with the first ground-based interferometers (such as LIGO, GEO, and Virgo) contribute to the astrophysical understanding of the sources. Double neutron

stars (DNS) and their inspiral due to GW emission represent the primary target source. This is primarily because they are known to exist in the Galaxy, with the Hulse-Taylor binary and the binary pulsar (Burgay et al. 2003) being the staples of this class of binary compact objects. Double compact objects with black hole (BH) components (i.e., BH-NS and BH-BH) have not yet been discovered in nature, but our current understanding of binary star evolution naturally predicts such BH binaries that would coalesce within a Hubble time (Belczynski et al. 2002b; Brown 1995; Portegies Zwart & Yungelson 1998; O'Shaughnessy et al. 2005b; Hurley et al. 2002; Portegies Zwart & Verbunt 1996; Fryer et al. 1998; Bethe & Brown 1999).

The sample of known DNS in the Galaxy has been very well studied and monitored since their discovery and as a result there is a wealth of information about their physical properties. This observational sample provides us with a unique opportunity to investigate the evolutionary history of these systems and a number of studies have addressed this basic question from different points of view. Another way to address the question of the formation of double compact objects is to develop population synthesis models that follow the evolution of large ensembles of binaries. Such models allow the detailed study of evolutionary channels that lead to double compact object formation and assess their relative efficacy and the main binary evolution phases that affect the final properties of the binaries.

The calculation of inspiral rates for double compact objects and associated event rates for ground-based GW detectors lies at the center of research activity related to GW searches in the last decade. These calculations were pioneered by Phinney (1991) and Narayan et al. (1991). Since then, a number of studies have considered this problem and revised these initial results, following the methods introduced in 1991. A few years ago Kim et al. (2003) introduced a novel statistical method for the calculation of inspiral rates based on the observed systems (empirical estimates); this method allowed us for the first time to associate rate estimates with statistical and systematic uncertainties and to place these estimates on the basis of confidence levels. Inspiral rates have also been computed based on population synthesis calculations that explore a limited number of model assumptions. More recently O'Shaughnessy et al. (2005b) have combined the two methods and have used the empirical DNS estimates as constraints on model predictions, especially for BH binaries on which we have no direct guidance from observations.

In this paper we summarize our group's work in this area in the context of double compact object formation, their properties and inspiral rates and in connection to other studies that have appeared in the literature.

2 The Recent Evolutionary History of Known Close Double Neutron Stars

According to our current knowledge (for more details see Bhattacharya & van den Heuvel 1991; Brown 1995; Belczynski et al. 2002b; Tauris & van den Heuvel 2006), double neutron stars (DNSs) form from primordial binaries in which, possibly after some initial mass-transfer phase, both component stars have masses in excess of $\sim 8-12\,M_{\odot}$. After the primary explodes in a supernova (SN) explosion to form the first neutron star (NS), the binary enters a high-mass X-ray binary phase in which the NS accretes matter from the wind of its companion. The phase ends when the companion star evolves of the main sequence and engulfs the NS in its expanding envelope. The NS then spirals in towards the core of the companion until enough orbital energy is transferred to the envelope to expel it from the system. When the envelope is ejected, the binary consists of the NS and the stripped-down helium core of its former giant companion, orbiting each other in a tight orbit. If the NS is able to accrete during its rapid inspiral, a first "recycling" may take place during which it is spun up to millisecond periods. The helium star then evolves further until it, in turn, explodes and forms a NS. Depending on the mass of the helium star and the size of the orbit at the time of the explosion, the SN may be preceded by a second recycling phase when the helium star fills its Roche lobe and transfers mass to the NS (Belczyński & Kalogera 2001; Belczynski et al. 2002a,b).

In what follows in this section we use this basic evolutionary framework and the complete, up-to-date set of observational constraints (at the time of this writing) on three DNS Galactic systems to investigate the physical properties of progenitor binaries at the time of the second SN explosion. We primarily summarize the work presented in Willems et al. (2006) and Willems et al. (2004) with many comparisons to other published studies addressing similar questions.

2.1 PSR J0737-3039: The Double Pulsar

The recent discovery of the strongly relativistic binary pulsar (Burgay et al. 2003) which is also the first eclipsing double pulsar system found in our Galaxy (Lyne et al. 2004) has resparked the interest in the evolutionary history and formation of DNS systems (Willems & Kalogera 2004; Dewi & van den Heuvel 2004; Willems et al. 2004). Shortly after the discovery of PSR J0737-3039, Dewi & van den Heuvel (2004) and Willems & Kalogera (2004) independently derived that, right before the second SN explosion, the binary was so tight that the helium star must have been overflowing its critical Roche lobe. This conclusion, for the first time, strongly confirmed the above formation channel

for DNS binaries. The observed 22.7 ms pulsar (hereafter PSR J0737-3039A or pulsar A) then corresponds to the first-born NS, and its 2.8 s pulsar companion (hereafter PSR J0737-3039B or pulsar B) to the second-born NS.

The main properties of the double pulsar system and its component stars relevant to this investigation are summarized in Table 1 of Willems et al. (2006).

The kinematic properties of PSR J0737-3039 have undergone significant revision since Ransom et al. (2004) used interstellar scintillation measurements and inferred a velocity component perpendicular to the line-of-sight of $\sim 141\,\mathrm{km\,s^{-1}}$. Coles et al. (2005) derived a reduced velocity of $\sim 66\,\mathrm{km\,s^{-1}}$ by incorporating anisotropies of the interstellar medium in the interstellar scintillation model. This reduced velocity, however, strongly depends on the adopted anisotropy model. Kramer et al. (2005), on the other hand, used pulsar timing measurements to derive a firm model-independent upper limit of $30\,\mathrm{km\,s^{-1}}$ on the transverse velocity.

The kick imparted to pulsar B at birth is expected to tilt the orbital plane and misalign pulsar A's spin axis with respect to the post-SN orbital angular momentum axis (e.g., Kalogera 2000). The degree of misalignment depends on both the magnitude and the direction of the kick, and therefore yields a valuable piece of information on pulsar B's natal kick velocity. In Willems et al. (2004) we showed that for the pre- and post-SN orbital parameters compatible with all available observational constraints, misalignment angles between approximately 70° and 110° are highly unlikely. Manchester et al. (2005) derived observational constraints on the spin-orbit misalignment based on the stability of pulsar A's mean pulse profile over a time span of 3 years. The authors concluded the angle to be smaller than $\sim 60°$ or larger than $\sim 120°$, in agreement with the theoretical predictions of Willems et al. (2004). These misalignment limits inferred by Manchester et al. (2005) are incorporated in the list of available observational constraints.

Among the constraints inferred from observations, the most uncertain parameter affecting the reconstruction of the system's formation and evolutionary history is its age. Characteristic ages, defined as half the ratio of the spin period to the spin-down rate, are the most commonly adopted age estimators, but are known to be quite unreliable (e.g. Kramer et al. 2003). In the case of PSR J0737-3039, the spin evolution of pulsar B is furthermore very likely affected by torques exerted by pulsar A on pulsar B (Lyutikov 2004), adding to the uncertainties of its age. Lorimer et al. (2005) therefore derived an alternative age estimate by noting that, according to the standard DNS formation channel, the time expired since the end of pulsar A's spin-up phase should be equal to the time expired since the birth of pulsar B. By combining this property with a selection of different spin-down models, the authors derived a *most likely* age of 30-70 Myr, but were unable to firmly exclude younger and

older ages. A third age estimate can be obtained by assuming that pulsar A was recycled to the maximum spin rate and calculating the time required for it to spin down to the currently observed value. This so-called spin-down age provides an upper limit to the age of the system of 100 Myr (Burgay et al. 2003). In view of these uncertainties, we derive constraints on the formation and evolution of PSR J0737-3039 for three different sets of age assumptions: (i) $0 \leq \tau \leq 100$ Myr, (ii) $30 \leq \tau \leq 70$ Myr (the most likely age range derived by Lorimer et al. (2005)), and (iii) $\tau \simeq 50$ Myr (the characteristic age of pulsar B).

2.1.1 Basic assumptions and outline of the calculation

In the following subsections we use the presently known observational constraints to reconstruct the evolutionary history of PSR J0737-3039 and constrain its properties at the formation time of pulsar B. More specifically, our aim is to derive a probability distribution function (PDF) for the magnitude and direction of the kick velocity imparted to pulsar B at birth, the mass of pulsar B's progenitor immediately before it explodes in a SN explosion, and the orbital separation of the component stars right before the SN explosion. Other recent studies with similar goals include Piran & Shaviv (2006) and Stairs et al. (2006). Adopting the standard DNS formation channel, the progenitor of the double pulsar right before the formation of pulsar B, consists of the first-born NS, pulsar A, and the helium star progenitor of the second-born NS. Since the formation of the second NS is preceded by one or more mass-transfer phases, tidal forces can safely be assumed to circularize the orbit prior to the formation of pulsar B. In what follows, we refer to the times right before and right after the formation of pulsar B by pre-SN and post-SN, respectively. The analysis presented consists of four major parts.

Firstly, the motion of the system in the Galaxy is traced back in time up to a maximum age of 100 Myr. The goal of this calculation is to derive the position and center-of-mass velocity of the binary right after the formation of pulsar B, and use this information to constrain the kick imparted to it at birth. In order to determine possible birth sites, our analysis is supplemented with the assumptions that the primordial DNS progenitor was born close to the Galactic plane, and that the first SN explosion did not kick the binary too far out of it. The first assumption is conform with our current knowledge that massive stars form and live close to the Galactic plane (their typical scale height is $\simeq$ 50–70 pc). The second assumption on the other hand neglects a small fraction of systems formed with high space velocities (Pfahl et al. 2002; Belczynski et al. 2002b). Under these assumptions, the binary is still close to the Galactic plane at the formation time of pulsar B. Possible birth sites can thus be obtained by calculating the motion in the Galaxy backwards in time and looking for crossings of the orbit with the Galactic mid-plane. The times

in the past at which the plane crossings occur yield kinematic estimates for the age of the DNS, while comparison of the system's total center-of-mass velocity with the local Galactic rotational velocity at the birth sites yields the system's post-SN *peculiar* velocity.

Secondly, the orbital semi-major axis and eccentricity right after the SN explosion forming pulsar B are determined by integrating the equations governing the evolution of the orbit due to gravitational wave emission backwards in time. The integration is performed for each Galactic plane crossing found from the Galactic motion calculations. Since each crossing yields a different kinematic age, and thus a different endpoint of the reverse orbital evolution calculation, the post-SN parameters are a function of the considered Galactic plane crossing.

Thirdly, the conservation laws of orbital energy and angular momentum are used to map the post-SN binary parameters to the pre-SN ones. The mapping depends on the kick velocity imparted to pulsar B at birth and results in constraints on the magnitude and direction of the kick velocity, the mass of pulsar B's pre-SN helium star progenitor, and the pre-SN orbital separation. The pre-SN orbital eccentricity is assumed to be zero, as expected from strong tidal forces operating on the binary during the mass-transfer phase(s) responsible for spinning up pulsar A. The kick and pre- and post-SN binary parameters are then furthermore subjected to the requirements that they be consistent with the post-SN peculiar velocity obtained from the Galactic motion calculations and with the observationally inferred spin-orbit misalignment angle of pulsar A. The latter constraint requires the additional assumption that tidal forces align the pre-SN rotational angular momentum vector of pulsar A with the pre-SN orbital angular momentum vector.

Fourthly, the solutions of the conservation laws of orbital energy and angular momentum are weighted according to the likelihood that they lead to the system's currently observed position and velocity in the Galaxy. A PDF of the admissible kick velocity and progenitor parameters is then constructed by binning the solutions in a multi-dimensional "rectangular" grid. The maximum of the resulting PDF yields the most likely magnitude and direction of the kick velocity imparted to pulsar B at birth, mass of pulsar B's pre-SN helium star progenitor, and pre-SN orbital separation. We also investigate the sensitivity of the PDF to the adopted assumptions by systematically varying the underlying assumptions, such as, e.g., the age and the magnitude of the transverse systemic velocity component.

2.1.2 Kinematic age and history

Tracing the motion of PSR J0737-3039 back in time requires the knowledge of both its present-day position and 3-dimensional space velocity. Unfortunately, no method is presently available to measure radial velocities of DNSs, so that the knowledge of their space velocity is limited to the component perpendicular to the line-of-sight (transverse velocity). At the time of this analysis, only an upper limit was available for the double pulsar [1] . The direction of the motion in the plane perpendicular to the line-of-sight is still unknown. Therefore we explore the system's kinematic history in terms of two unknown parameters: (i) the radial component V_r of the present-day systemic velocity, and (ii) the orientation Ω of the transverse velocity in the plane perpendicular to the line-of-sight. Since the results presented in this paper do not depend on the exact definition of Ω, we refer the reader to Willems et al. (2004) for a more detailed discussion and definition. We calculate the motion of the system in the Galaxy backwards in time using the Galactic potential of Carlberg & Innanen (1987) with updated model parameters derived by Kuijken & Gilmore (1989). Since at the time of the analysis kinematical constraints provided only an upper limit of $30\,\mathrm{km}\,s^{-1}$ on the transverse systemic velocity, and the calculation of the past orbit requires precise starting values for both the present-day position and the present-day velocity, we calculate the motion backwards in time for two specific velocities: $V_t = 10\,\mathrm{km\,s^{-1}}$ and $V_t = 30\,\mathrm{km\,s^{-1}}$ in what follows.

The number of Galactic plane crossings associated with each V_r and Ω, within the adopted age limit of 100 Myr, can be anywhere between 1 and 5. The times in the past at which the system crosses the Galactic plane furthermore yield kinematic estimates for the age of the DNS, while subtraction of the Galactic rotational velocity from the total systemic velocity at the birth sites yields the peculiar velocity right after the formation of pulsar B.

Since there are no a priori constraints on the magnitude of the radial velocity, we examine the effect of incorporating large radial velocities in the analysis by weighting each considered radial velocity according to a pre-determined radial velocity distribution. For this purpose, we performed a population synthesis study of Galactic DNSs, including their kinematic evolution in the potential of Carlberg & Innanen (1987). Theoretical radial velocity distributions are then obtained by taking a snapshot of the population at the current epoch and determining the radial velocity for each DNS in the sample. The resulting PDFs are found to be represented well by Gaussian distributions with means of $0\,\mathrm{km\,s^{-1}}$ and velocity dispersions of 60–200 $\mathrm{km\,s^{-1}}$, depending on the adopted population synthesis assumptions. For comparison, we also consider a uniform radial velocity distribution in which all radial velocities between -1500 $\mathrm{km\,s^{-1}}$ and $1500\,\mathrm{km\,s^{-1}}$ are equally probable. For the other unknown parameter, the

[1] At present a measurement of $10\,\mathrm{km\,s^{-1}}$ has been reported by Kramer et al. (2006).

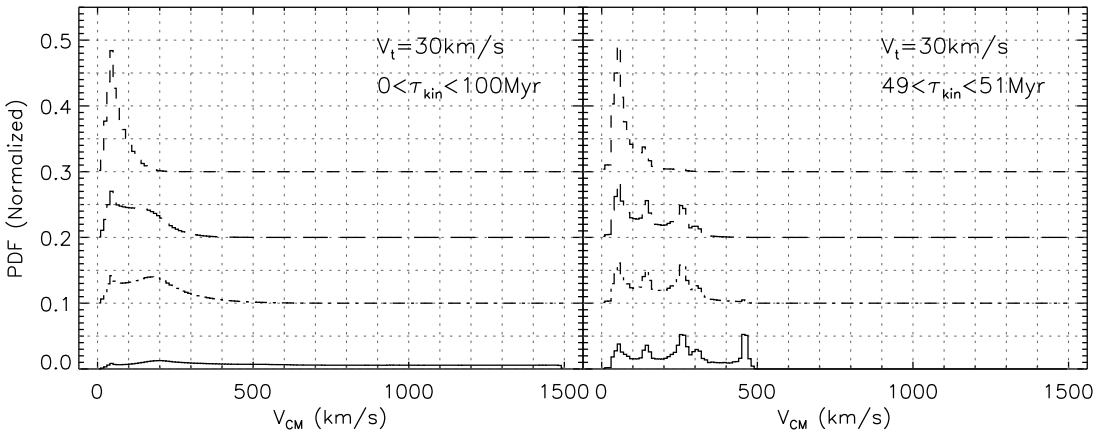

Fig. 1. Distribution of post-SN peculiar velocities for a present-day transverse velocity of $30\,\mathrm{km\,s^{-1}}$, kinematic ages ranges of 0–100 Myr and 49–51 Myr, and radial velocity distributions varying from a uniform distribution (solid line) to Gaussian distributions with velocity dispersions of $60\,\mathrm{km\,s^{-1}}$ (long-dashed line), $130\,\mathrm{km\,s^{-1}}$ (short-dashed line), and $200\,\mathrm{km\,s^{-1}}$ (dash-dotted line). For clarity, the PDFs are offset from each other by an arbitrary amount.

orientation angle Ω of the transverse velocity component in the plane perpendicular to the line-of-sight, we assume a uniform distribution between 0° and 360°.

In Fig. 1, the distribution of post-SN peculiar velocities obtained by tracing the motion of PSR J0737-3039 in the Galaxy back in time is shown for a present-day transverse velocity component of $30\,\mathrm{km\,s^{-1}}$, and kinematic age ranges of 0-100 Myr and 49-51 Myr. These probability distributions are calculated considering weights according to (i) the probability that the system has a present-day radial velocity V_r (assumed to be distributed according to a uniform or a Gaussian distribution), (ii) the transverse velocity has a direction angle Ω (assumed to be uniformly distributed), and (iii) the system is found at its current position in the Galaxy (determined by the time the system spends near its current position divided by its kinematic age).

Here, we determine the probability of finding the system at its current position in the Galaxy in three dimensions (i.e., besides the vertical distance to the Galactic plane, we also consider the radial and azimuthal position in the plane). For this purpose, we determine the time the system spends in a sphere with radius R centered on its current location for all V_r- and Ω-values considered for the derivation of the possible birth sites. The probability to find the system near its current position is then determined as the time it spends in this sphere divided by its age. For the latter, we adopt the kinematic ages obtained by tracing the motion of the system backwards in time, so that the probability of finding the system near its current position depends on the radial velocity V_r, the proper motion direction Ω, and the Galactic plane crossing considered along the orbit associated with V_r and Ω. We per-

formed some test calculations to successfully verify that the results based on the thus determined probabilities are insensitive to the adopted value of R, as long as it is sufficiently small for the sphere to represent a local neighborhood near the system's current position. For the results presented in this paper we, somewhat arbitrarily, choose $R = 50\,\mathrm{pc}$.

Ultimately, the probability that, for a given pair of V_r and Ω, the post-SN peculiar velocity of the binary is equal to V_{CM} is given by

$$P\left(V_{\mathrm{CM}}|V_r,\Omega\right) \propto \sum_{i=1}^{N(V_r,\Omega)} \frac{T\left(V_r,\Omega\right)}{\tau_{\mathrm{kin},i}\left(V_r,\Omega\right)} \lambda_i\left(V_r,\Omega\right), \tag{1}$$

where $N(V_r,\Omega)$ is the number of Galactic plane crossings associated with V_r and Ω, $T(V_r,\Omega)$ is the time the system spends near its current position for the orbit associated with V_r and Ω, and $\tau_{\mathrm{kin},i}\left(V_r,\Omega\right)$ is the kinematic age corresponding to the i-th plane crossing associated with V_r and Ω. The factor $\lambda_i\left(V_r,\Omega\right)$ is equal to 1 when the i-th plane crossing along the orbit associated with V_r and Ω yields a post-SN peculiar velocity equal to V_{CM}, and equal to 0 otherwise. The total probability that the post-SN peculiar velocity of the binary is equal to V_{CM} is then obtained by integrating Eq. (1) over all possible values of V_r and Ω:

$$P\left(V_{\mathrm{CM}}\right) \propto \int_{\Omega}\int_{V_r} P\left(V_{\mathrm{CM}}|V_r,\Omega\right) P\left(V_r\right) P\left(\Omega\right) dV_r\, d\Omega. \tag{2}$$

Here $P(V_r)$ is the probability distribution of the unknown radial velocity V_r, and $P(\Omega)$ the probability distribution of the unknown proper motion direction Ω in the plane perpendicular to the line-of-sight.

For ages of 0-100 Myr, post-SN peculiar velocities up to $100\,\mathrm{km\,s^{-1}}$ are likely for all four radial velocity distributions. The highest post-SN peculiar velocities are found for the Gaussian radial velocity distributions with velocity dispersions of $130\,\mathrm{km\,s^{-1}}$ and $200\,\mathrm{km\,s^{-1}}$ (V_{CM} values remain likely up to 200–$300\,\mathrm{km\,s^{-1}}$) and the uniform radial velocity distribution (V_{CM} values follow an almost flat distribution from $300\,\mathrm{km\,s^{-1}}$ to $1500\,\mathrm{km\,s^{-1}}$). For ages of 49-51 Myr, the post-SN peculiar velocity distributions all have a peak at $50\,\mathrm{km\,s^{-1}}$. In the case of the uniform radial velocity distribution and the Gaussian distributions with velocity dispersions of $130\,\mathrm{km\,s^{-1}}$ or $200\,\mathrm{km\,s^{-1}}$, additional peaks of almost equal height occur at even higher post-SN peculiar velocities. Similar conclusions apply to the post-SN peculiar velocity distributions obtained for a present-day transverse velocity component of $10\,\mathrm{km\,s^{-1}}$. Despite the small lower limit on the present-day *transverse* systemic velocity, a wide range of non-negligible post-SN peculiar velocities is thus possible. We note however that the distributions shown here incorporate all possible post-SN peculiar

velocities obtained from tracing the motion of the system backwards in time and that some of these may require SN kicks and mass loss that are incompatible with the observational constraints on the orbital elements and component masses of the double pulsar.

2.1.3 Progenitor constraints

After the formation of pulsar B, the evolution of the system is expected to be driven exclusively by the emission of gravitational waves. We use the differential equations derived by Junker & Schäfer (1992) which are valid up to 3.5 post-Newtonian order of approximation, and find the resulting post-SN orbital separation A to be always between $1.26\,R_\odot$ and $1.54\,R_\odot$, and the post-SN orbital eccentricity e between 0.088 and 0.12. Since the kinematic ages are functions of the radial velocity V_r, the proper motion direction Ω, and the Galactic plane crossing considered along the past orbit associated with V_r and Ω, the particular values of A and e associated with a given $\tau_{\rm kin}$ are also functions of these variables.

The pre- and post-SN binary parameters and the kick velocity imparted to pulsar B at birth are related by the conservation laws of orbital energy and angular momentum. For a circular pre-SN orbit, the relations can be found in (Hills 1983; Brandt & Podsiadlowski 1995; Kalogera 1996; Fryer & Kalogera 1997; Kalogera & Lorimer 2000).

The requirement that these equations permit real solutions for the kick magnitude V_k, the kick orientation angles θ, ϕ, the NS progenitor mass M_0, and the pre-SN orbital semi-major axis A_0, imposes constraints on all of these parameters. For a mathematical formulation of these constraints, we refer to Eqs. (21)–(27) in Willems et al. (2005), and references therein (a more compact description can also be found in Willems & Kalogera (2004) and Willems et al. (2004). We here merely recall that the constraints express that: (i) the binary components must remain bound after the SN explosion, (ii) the pre- and post-SN orbits must pass through the instantaneous position of the component stars at the time of the SN explosion, and (iii) there is a lower and upper limit on the degree of orbital contraction or expansion associated with a given amount of mass loss and a given SN kick.

Besides the changes in the orbital parameters and the mass of the exploding star, the SN explosion also imparts a kick velocity to the binary's center of mass and tilts the post-SN orbital plane with respect to the pre-SN one. The center-of-mass velocity and tilt angle add additional constraints on the solutions of the conservation laws of orbital energy and angular momentum.

The constraints on the progenitor of PSR J0737-3039 resulting from the dynamics of asymmetric SN explosions arise solely from tracing the evolution

of the current system properties backwards in time. The pre-SN orbital separations and pulsar B progenitor masses found this way are, however, not necessarily accessible through the currently known DNS formation channels. Further constraints on the progenitor of pulsar B can therefore be obtained from stellar and binary evolution calculations.

Firstly, a lower limit on the mass of pulsar B's pre-SN progenitor is given by the requirement that the star must be massive enough to evolve into a NS rather than a white dwarf. According to our current understanding of helium star evolution, the minimum helium star mass required for NS formation is 2.1–2.8 $M_\odot$ (Habets 1986; Tauris & van den Heuvel 2006). The actual helium star minimum mass is, however, still considerably uncertain due to the poorly understood evolution of massive stars and possible interactions with close binary companions.

We impose a lower limit of 2.1 $M_\odot$ on the mass of pulsar B's pre-SN helium star progenitor. However, in the light of recent suggestions that the progenitor of pulsar B may have been significantly less massive than the conventional lower limit of 2.1 $M_\odot$, we also explore the possibility of progenitor masses as low as pulsar B's present-day mass of 1.25 $M_\odot$ (Piran & Shaviv 2005a; Podsiadlowski et al. 2005). Unless our current understanding of helium star evolution is seriously flawed, this scenario implies that the progenitor of pulsar B must have lost a significant amount of mass (at least $\sim 0.7\,M_\odot$) after it had already established a sufficiently massive core to guarantee the occurrence of a future SN explosion. We note that this possibility is included in the binary population synthesis calculations used to derive the adopted theoretical DNS radial-velocity distributions.

Secondly in Willems & Kalogera (2004), we showed that the pre-SN binary was so tight ($1.2\,R_\odot \lesssim A_0 \lesssim 1.7\,R_\odot$) that the helium star progenitor of pulsar B must have been overflowing its Roche lobe at the time of its SN explosion (see also Dewi & van den Heuvel 2004). An upper limit on the progenitor mass is therefore given by the requirement that this mass-transfer phase be dynamically stable (otherwise the components would have merged and no DNS would have formed). Based on the evolutionary tracks for NS + helium star binaries calculated by Ivanova et al. (2003), we adopt an upper limit of 3.5 on the mass ratio of the pre-SN binary to separate dynamically stable from dynamically unstable Roche-lobe overflow (see also Dewi et al. 2002; Dewi & Pols 2003).

2.1.4 The most likely kick velocity and progenitor properties

The most likely kick velocity and progenitor parameters obtained from the procedure outlined in the previous sections are summarized in Table IV of (Willems et al. 2006). The most likely pulsar B kick velocity is smaller than

$50\,\mathrm{km\,s^{-1}}$ only when the transverse velocity component has a magnitude of $10\,\mathrm{km\,s^{-1}}$, the minimum helium star mass required for NS formation is allowed to be as low as $1.25\,M_\odot$, and the age of the system is assumed to be between 30 and 70 Myr. *All other models* yield most likely kick velocities of 50–180 $\mathrm{km\,s^{-1}}$. When a minimum pre-SN helium star mass of $2.1\,M_\odot$ is imposed, the kicks are always strongly favored to be directed opposite to the helium star's pre-SN orbital motion (most likely $\cos\theta \simeq -0.90 \pm 0.05$). When the constraint on the minimum pre-SN helium star mass is relaxed, the most likely kick direction can shift significantly and can even become perpendicular to the helium star's pre-SN orbital velocity. Allowing pre-SN helium star masses down to $1.25\,M_\odot$ furthermore always leads to most likely progenitor masses of $1.3 - 2.0\,M_\odot$, *except* when $V_t = 10\,\mathrm{km\,s^{-1}}$, the age of the system is between 0 and 100 Myr, and the radial velocities are distributed uniformly or according to a Gaussian with a velocity dispersion of $200\,\mathrm{km\,s^{-1}}$. In the latter cases, the most likely progenitor masses are 2.5–2.7 $M_\odot$.

In summary, while small kick velocities of just a few tens of $\mathrm{km\,s^{-1}}$ could be favored for some models, the majority of the models yields most likely values of 50–180 $\mathrm{km\,s^{-1}}$. Progenitor masses below $2.1\,M_\odot$ are furthermore not required to explain the system properties, although they are generally favored when helium stars below $2.1\,M_\odot$ are still assumed to be viable NS progenitors. We note though that the results presented are based on the assumption that all kick velocity magnitudes V_k are equally probable. This assumption is inconsistent for models using the Gaussian radial velocity distributions based on population synthesis calculations of coalescing DNSs. In particular, these calculations all adopt a Maxwellian rather than a uniform kick velocity distribution. In all cases, weighing the kick velocities according to the Maxwellian underlying the derivation of the radial velocity distributions would, however, shift the most likely kick velocities to higher V_k values. This reinforces our conclusion that the presently known observational constraints not necessarily disfavor kick velocity magnitudes of $100\,\mathrm{km\,s^{-1}}$ or more.

2.1.5 Confidence limits on the kick velocity and progenitor parameters

For illustration, some representative 1-D PDFs used for the calculation of the confidence limits in the case of a present-day transverse velocity component of $10\,\mathrm{km\,s^{-1}}$ are shown in Fig. 2. Panels (a)–(c) show the kick velocity distributions resulting from different present-day radial velocity distributions for ages ranges of 0-100 Myr and 49-51 Myr, and minimum pre-SN helium star masses of $1.25\,M_\odot$ and $2.1\,M_\odot$. For a given age range and minimum pre-SN helium star mass, the PDFs show a peak which is most pronounced when a Gaussian radial velocity distribution with a velocity dispersion of $60\,\mathrm{km\,s^{-1}}$ is considered, and which widens with increasing radial velocity dispersions. When the age is assumed to be 0-100 Myr and the minimum pre-SN helium star mass

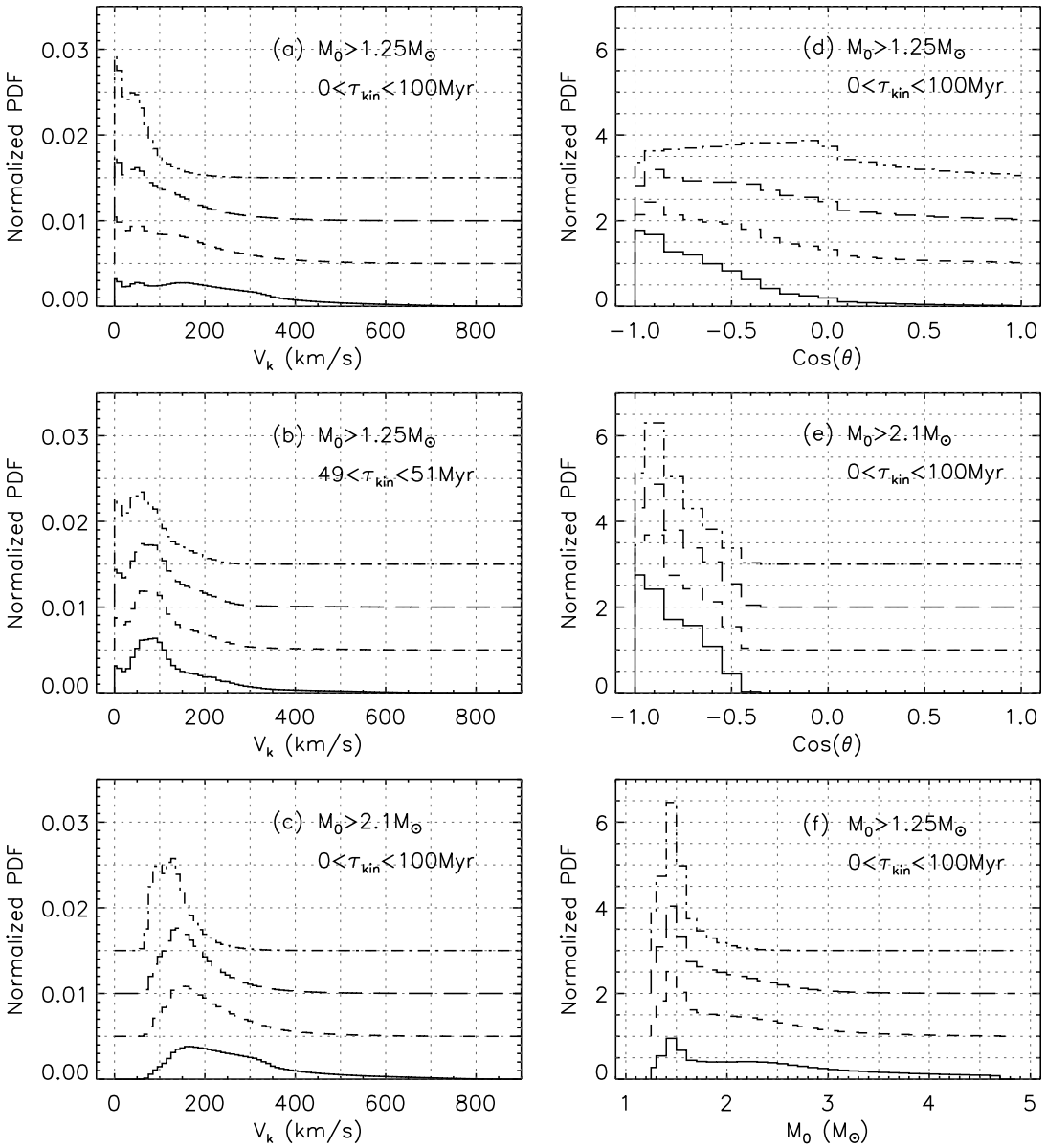

Fig. 2. One-dimensional PDFs illustrating some of the dependencies of the derived pulsar B kick velocity and progenitor properties on the adopted model assumptions. All plots are for a present-day transverse velocity of $10\,\mathrm{km\,s^{-1}}$. Solid lines correspond to uniform radial velocity distributions and dashed lines to Gaussian distributions with velocity dispersions of $60\,\mathrm{km\,s^{-1}}$ (long-dashed lines), $130\,\mathrm{km\,s^{-1}}$ (short-dashed line), and $200\,\mathrm{km\,s^{-1}}$ (dash-dotted line). For clarity, the PDFs are offset from each other by an arbitrary amount. Panels (a)–(c) show the distributions of kick velocity magnitudes V_k, panels (d)–(e) the distributions of kick direction cosines $\cos\theta$, and panel (f) the distributions of pre-SN helium star masses M_0.

$1.25\,M_\odot$, there is a clear tendency for the 1-D PDFs to favor kick velocities of $50\,\mathrm{km\,s^{-1}}$ or less (although this becomes significantly less pronounced with increasing radial velocity dispersions). This trend shifts towards favoring kick velocities of 50–100 $\mathrm{km\,s^{-1}}$ when the age range is narrowed to 49-51 Myr. Moreover, when the age range is kept fixed at 0-100 Myr, but the minimum pre-SN helium star mass is increased to $2.1\,M_\odot$, the favored range of kick velocities shifts to 100–150 $\mathrm{km\,s^{-1}}$. In the latter case, the kick velocity is furthermore always required to be larger than $\sim 60\,\mathrm{km\,s^{-1}}$ (see also Willems & Kalogera 2004; Willems et al. 2004).

Panel (f), finally, shows the distribution of possible pre-SN progenitor masses for different present-day radial velocity distributions, DNS ages of 0-100 Myr, and a minimum pre-SN helium star mass of $1.25\,M_\odot$. The distributions all favor progenitor masses of 1.4–1.5 $M_\odot$, with the preference for this mass range being strongest for present-day radial velocity distributions with small radial velocity dispersions. Distribution functions for a minimum pre-SN helium star mass of $2.1\,M_\odot$ look practically the same as the ones displayed panel (f) if they were cut off at $2.1\,M_\odot$.

2.1.6 Summary and concluding remarks

One of the results of the above analysis is that marginalizing the full five-dimensional progenitor PDF to 1-D or 2-D distributions for the pulsar B kick velocity and progenitor mass has a major effect on the determination of their most likely values. When the full multi-dimensional PDF is examined, it is clear that although some sets of prior assumptions indeed favor low kick velocities and low progenitor masses the majority of the models favor kick velocities of 50–180 $\mathrm{km\,s^{-1}}$ and progenitor masses of 1.45–2.75 $M_\odot$.

In particular, if the transverse systemic velocity is assumed to be 10 km/s and helium stars less massive than $2.1\,M_\odot$ are assumed to be viable NS progenitors, the most likely progenitor mass can vary from $1.35\,M_\odot$ to $2.65\,M_\odot$, depending on the assumed systemic age and radial velocity distribution. Hence, whether progenitor masses greater than $2.1\,M_\odot$ are statistically likely or unlikely depends strongly on the adopted prior assumptions (cf. Piran & Shaviv 2005a,b). Most likely progenitors with $M_0 < 2.1\,M_\odot$ can furthermore also be associated with kick velocities of up to $100\,\mathrm{km\,s^{-1}}$. Stairs et al. (2006) recently arrived at similar conclusions based on updated proper motion measurements by Kramer et al. (2006). The updated measurements yield a proper motion of 10 km/s in a direction nearly parallel to the plane of the Galaxy.

We also find that the proximity of PSR J0737-3039 to the Galactic plane and the small proper motion do not pose stringent constraints on the kick velocity and progenitor mass of pulsar B. Instead, the constraints are predominantly

determined by the orbital dynamics of asymmetric SN explosions. This is in contrast to the conclusions of Piran & Shaviv (2005a) and Piran & Shaviv (2005b) who emphasize that the proximity of the double pulsar to the Galactic plane implies that pulsar B most likely received only a small kick at birth and that its progenitor most likely had mass of $\sim 1.45\,M_\odot$.

Hence, based on the currently available observational constraints, a wide range of progenitor and kick velocity properties are favored for PSR J0737-3039B. In particular, the constraints are compatible with a conventional hydrodynamical or neutrino-driven SN explosion from a helium star more massive than $2.1\,M_\odot$ (Habets 1986; Tauris & van den Heuvel 2006), as well as an electron-capture SN from a helium star less massive than $2.5\,M_\odot$ (Nomoto 1984, 1987). Podsiadlowski et al. (2005) have speculated that the electron-capture SN mechanism may be typical for close binaries and that it may be accompanied by much smaller kicks than hydrodynamical or neutrino-driven SN explosions. Consequently, if pulsar B is formed through an electron capture SN and if electron capture SNe are accompanied by small kicks, the mass of pulsar B's pre-SN helium star progenitor must be smaller than $2.1\,M_\odot$ (otherwise the kick is always larger than $\sim 60\,\mathrm{km\,s^{-1}}$). Since it is unlikely that future observations will lead to new constraints on the smallest possible pulsar B progenitor mass, further insight to the formation mechanism of pulsar B should be sought in core-collapse simulations of low-mass ($\lesssim 2.1\,M_\odot$) helium stars and population synthesis studies of PSR J0737-3039-type binaries and their progenitors.

2.2 PSR B1534+12

The relativistic binary radio pulsar PSR B1534+12 too has an accurately measured proper motion with a known direction in right ascension and declination, so that its kinematic history and progenitor constraints *depend only on the unknown radial velocity* V_r. In order to derive these constraints, we adopt the spin-down age $\tau_b = 210\,\mathrm{Myr}$ as an upper limit to the age of the system. The other physical parameters of PSR B1534+12 relevant to the derivation are summarised in Table 1 of Willems et al. (2004).

Following the same arguments as for PSR J0737-3039, we assume that the progenitor of PSR B1534+12 was close to the Galactic plane at the time of the second SN explosion and that its pre-SN systemic velocity was almost entirely due to Galactic rotation. The possible birth sites of the DNS are then obtained by tracing the Galactic motion of the system backwards in time as a function of the unknown radial velocity V_r. We find that, within the imposed age limit of 210 Myr, no Galactic plane crossings occur when $V_r \gtrsim 250\,\mathrm{km\,s^{-1}}$, whereas up to four crossings may occur when $V_r \lesssim 250\,\mathrm{km\,s^{-1}}$. Since four

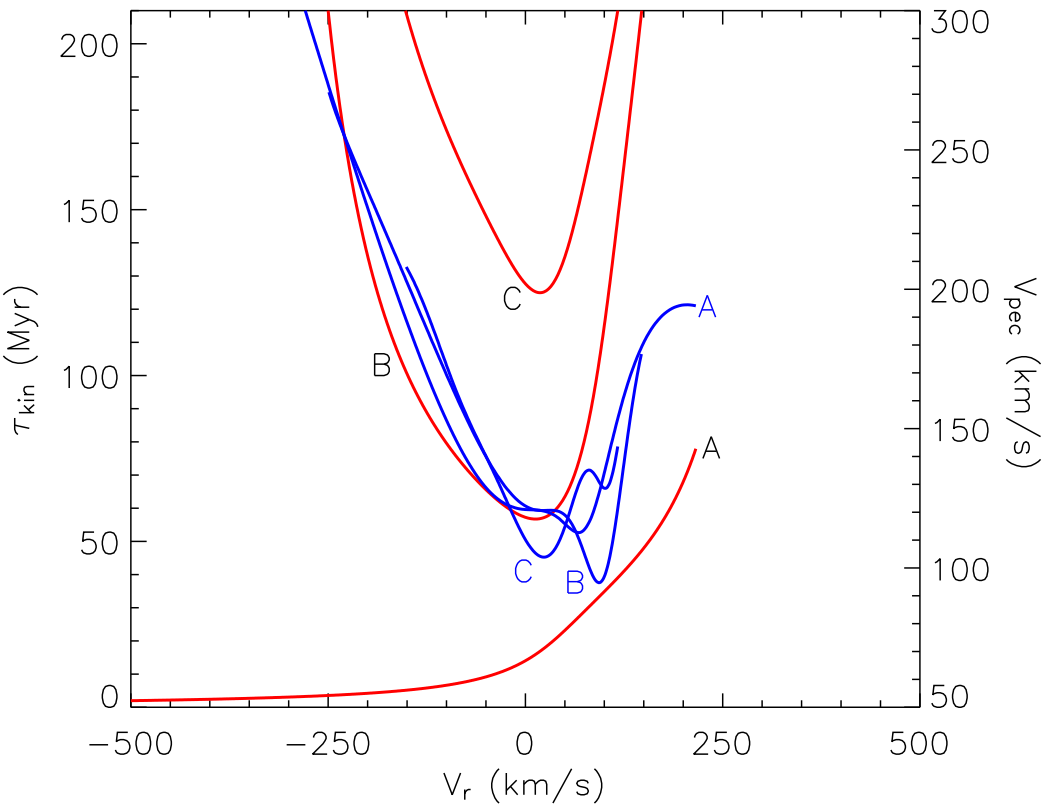

Fig. 3. Variations of the kinematic age (left-hand axis) and post-SN peculiar velocity (right-hand axis) of PSR B1534+12 as a function of the unknown radial velocity V_r, for cases A, B, and C. The kinematic ages are represented by red lines and the peculiar velocities by blue lines.

disk crossings only occur for relatively few and rather fine-tuned Galactic trajectories, we leave these cases aside and focus on the possible birth sites associated with the first (case A), second (case B), and third (case C) Galactic plane crossings.

The kinematic ages and post-SN peculiar velocities associated with the Galactic plane crossings are shown in Fig. 3 as functions of the radial velocity V_r. Case A gives rise to a wide range of ages between $\simeq 1$ Myr and 210 Myr, and peculiar velocities between 110 km s^{-1} and 1500 km s^{-1}. Cases B and C, on the other hand, yield kinematic ages of *at least* $\simeq 55$ Myr and $\simeq 125$ Myr; and post-SN peculiar velocities of 90–270 km s^{-1} and 100–220 km s^{-1}, respectively.

The post-SN orbital separation A and orbital eccentricity e at the times of Galactic disk crossings are obtained by numerical integration backwards in time of the equations governing the evolution of the orbit under the influence of gravitational radiation. The resulting post-SN orbital parameters range from $A = 3.28\,R_\odot$ and $e = 0.274$ when $\tau_{kin} = 0$ Myr to $A = 3.36\,R_\odot$ and $e = 0.282$ when $\tau_{kin} = 210$ Myr. These post-SN orbital parameters together with the post-SN peculiar velocities impose constraints on the pre-SN progenitor of

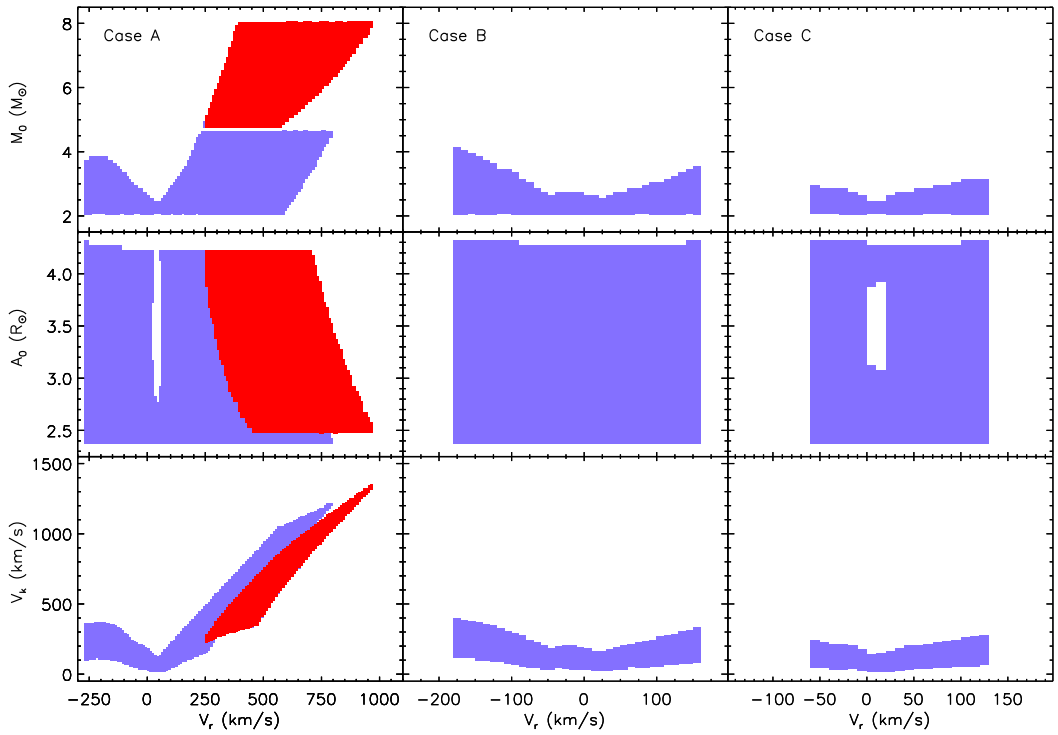

Fig. 4. Limits on the pre-SN progenitor of PSR B1534+12 and on the kick velocity imparted to the last-born NS. The left-hand panels show the constraints for case A, the middle panels for case B, and the right-hand panels for case C. Red regions correspond to solutions for which the pre-SN binary is detached, while blue regions indicate the additional solutions associated with mass-transferring systems.

PSR B1534+12. These are derived in a similar way as for the progenitor of PSR J0737-3037 (except that the problem depends on only one free parameter, V_r). The results of our analysis are summarized in Fig. 4.

Based on the observational constraints available in 2004, PSR B1534+12 may have been detached as well as semi-detached at the time the second NS was born. In order to illustrate this, the solutions for which no mass transfer takes place at the time of the second SN explosion are indicated by the red regions in Fig. 4, while the blue regions indicate the *additional* solutions that become accessible when the possibility of mass transfer is taken into account. For the latter solutions we adopt the same assumption as before that the system may survive the mass transfer phase and form a DNS only if the mass ratio is smaller than 3.5 (e.g., Ivanova et al. 2003).

For case A disk crossings, detached pre-SN binary configurations exist only for $V_r \lesssim -250\,\mathrm{km\,s^{-1}}$. For larger radial velocities, the system is always undergoing mass transfer from the progenitor of the second-born NS to the first-born NS. In this analysis, the pre-SN mass of the helium star forming the second NS is constrained within $2.1\,M_\odot - 8\,M_\odot$. The lower limit again corresponds to the lowest mass for which a helium star is expected to form a NS instead of a

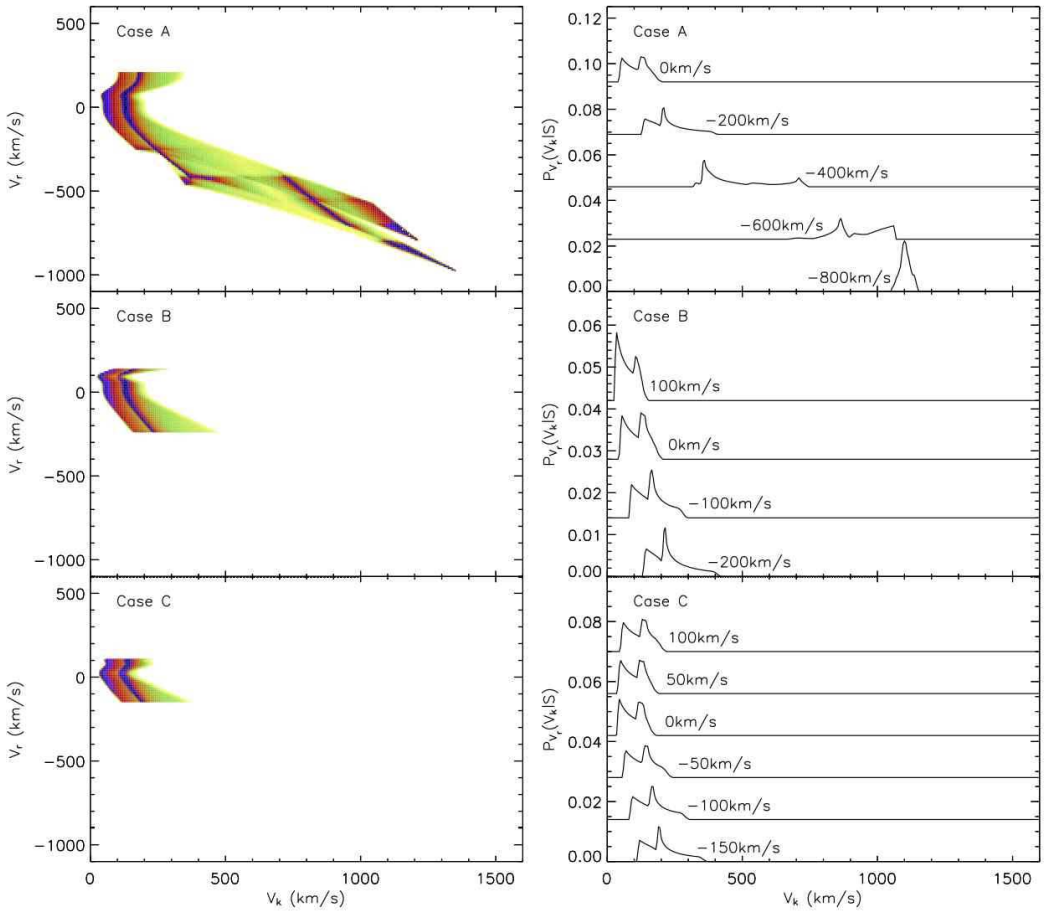

Fig. 5. Probability distribution functions of the magnitude of the kick velocity imparted to PSR B1534+12's companion at the time of its formation, for cases A, B, and C. The left panels show the entire set of PDFs associated with all admissible Vr-values by means of a linear color scale that varies over yellow, green, orange, red, and blue with increasing PDF values, while the right panels show the PDFs associated with some specific Vr-values. For clarity, the curves in the right panels are offset from each other by an arbitrary amount.

white dwarf, while the upper limit corresponds to the highest mass for which a helium star is expected to form a NS rather than a black hole (see, e.g., Fig. 1 in Belczynski et al. 2002b and Table 16.4 in Tauris & van den Heuvel 2006). The divide between the red and blue regions at $4.7\,M_\odot$ corresponds to the adopted critical mass ratio of 3.5 for dynamically stable mass transfer. The allowed mass range of pre-SN helium star masses is most constrained for $|V_r| \lesssim 200\,\mathrm{km\,s^{-1}}$ when $2.1\,M_\odot \lesssim M_0 \lesssim 4\,M_\odot$. Lower and upper limits on the pre-SN orbital separation are given by $2.4\,R_\odot$ and $4.3\,R_\odot$.

The behavior of the kick-velocity magnitude is similar as for PSR J0737-3039: the kick velocity increases with increasing absolute values of V_r and, for a given radial velocity, it is generally constrained to an interval that is less than

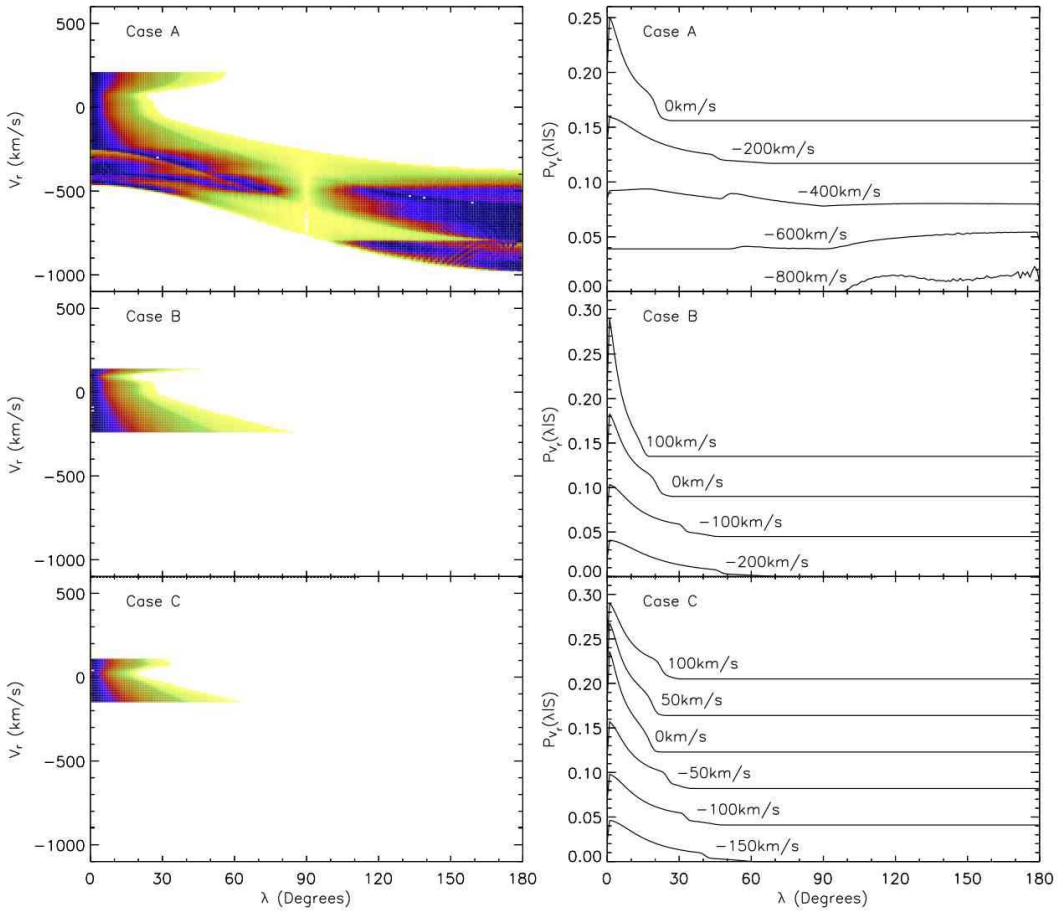

Fig. 6. Probability distribution functions for the misalignment angle λ between PSR B1534+12's spin axis and the post-SN orbital angular momentum axis, for cases A, B, and C (cf. Fig. 5 for more details).

$\simeq 600\,\mathrm{km\,s^{-1}}$ wide. Solutions for which the pre-SN helium star is overflowing its Roche lobe furthermore allow for somewhat higher kick velocities than solutions for which the helium star fits within its critical Roche lobe. These higher kick velocities are associated with the smaller orbital separations that become accessible for mass-transferring progenitors. When all possible pre-SN binary configurations are considered, the kick velocity magnitudes range from $45\,\mathrm{km\,s^{-1}}$ to $1350\,\mathrm{km\,s^{-1}}$. When configurations for which the helium star is overflowing its Roche lobe are excluded, the range narrows to $230\,\mathrm{km\,s^{-1}} \lesssim V_k \lesssim 1350\,\mathrm{km\,s^{-1}}$, so that the minimum required kick velocity is higher than when the possibility of Roche-lobe overflow is taken into account. The larger minimum kick velocity is required to compensate the larger effect of the mass lost from the system during the SN explosion: since the minimum M_0 for these systems is $4.7\,M_\odot$, at least 57% of the total pre-SN mass is lost from the system.

For case B disk crossings, almost all allowed pre-SN binary configurations

imply that the helium star progenitor of the second-born NS is overflowing its Roche lobe at the time of its SN explosion. The mass of the helium star is constrained to $2.1\,M_\odot \lesssim M_0 \lesssim 4.9\,M_\odot$, the pre-SN orbital separation to $2.4\,R_\odot \lesssim A_0 \lesssim 4.3\,R_\odot$, and the kick-velocity magnitude to $30\,\mathrm{km\,s^{-1}} \lesssim V_k \lesssim 475\,\mathrm{km\,s^{-1}}$. If the helium star fits within its critical Roche lobe at the time of its SN explosion, the constraints become $M_0 \approx 4.8\,M_\odot$, $A_0 \approx 4.2\,R_\odot$, $V_k \approx 240\,\mathrm{km\,s^{-1}}$.

Case C disk crossings, finally, yield no detached solutions for the progenitor of PSR B1534+12. The constraints for this case are similar to those found for case B, except that the mass M_0 is always smaller than $\simeq 4\,M_\odot$ and the kick velocity V_k is always smaller than $370\,\mathrm{km\,s^{-1}}$.

The constraints derived above may again be used to derive probability distribution functions for the magnitude V_k of the kick velocity imparted to the second-born NS and for the misalignment angle λ between the spin-axis of the first-born NS and the post-SN orbital angular momentum axis. We note that, unlike the PDFs derived for the double pulsar, the PDFs presented in this section do not incorporate probability distributions for V_r obtained from theoretical population synthesis calculations, nor do they incorporate the probability of finding the system at its current place in the Galaxy. The resulting PDFs are presented in Figs. 5 and 6. For radial velocities of only a few $100\,\mathrm{km\,s^{-1}}$, the kick-velocity distributions show two closely spaced and fairly evenly matched peaks between $V_k \simeq 50\,\mathrm{km\,s^{-1}}$ and $V_k \simeq 250\,\mathrm{km\,s^{-1}}$. For higher radial velocities, relevant only to case A, the peak(s) shift to larger kick velocities up to a maximum of $\simeq 1350\,\mathrm{km\,s^{-1}}$. The tilt-angle distributions, on the other hand, favor misalignment angles below 30° when $|V_r| \lesssim 200\,\mathrm{km\,s^{-1}}$ and above below 100° when $|V_r| \gtrsim 600\,\mathrm{km\,s^{-1}}$. For case A disk crossings, tilt angles close to $\lambda \approx 90°$ are furthermore strongly disfavored regardless of the value of the radial velocity. For case B and C disk crossings, tilt angles with non-vanishing probabilities are always smaller than 40°–50°. For kick velocities of less than $200\,\mathrm{km\,s^{-1}}$, the predictions in all three cases are in good agreement with the measurement of $\lambda = 25.0 \pm 3.8°$ by Stairs et al. (2004).

We conclude by noting that updated progenitor constraints by Thorsett et al. (2005) incorporating the tilt angle measured by Stairs et al. (2004) exclude the possibility that the progenitor was detached right before the SN explosion forming the second NS.

2.3 PSR B1913+16: The Hulse-Taylor Binary Pulsar

Besides the knowledge of the proper motion direction, PSR B1913+16 has the advantage that the misalignment angle between the pulsar's spin axis and the

pre-SN orbital angular momentum axis has been determined to be around $\simeq 20°$, corresponding to prograde rotation, or $\simeq 160°$, corresponding to retrograde rotation (Kramer 1998; Weisberg & Taylor 2002). Wex et al. (2000) used this information to derive constraints on the mass of the second-born NS's direct progenitor, on the pre-SN orbital separation, and on the magnitude and direction of the kick velocity imparted to the second-born NS at birth. In agreement with the then available numerical simulations of rapidly accreting neutron stars, the authors assumed that mass transfer from a helium star companion would cause the NS to collapse into a black hole and therefore excluded Roche-lobe overflowing helium stars as viable progenitors of the second-born NS. However, more recent calculations by Dewi et al. (2002), Ivanova et al. (2003), and Dewi & Pols (2003) show that NS binaries may survive a helium-star mass-transfer phase, provided that the ratio of the helium star's mass to the neutron star's mass is not too extreme (≤ 3.5). We therefore revise the constraints derived by Wex et al. (2000) in the light of this new information. The constraints on the tilt angle, for which we consider the values $\lambda = 18° \pm 6°$ and $\lambda = 162° \pm 6°$ are also imposed.

We look for possible birth sites of PSR B1913+16 by tracing the system's motion in the Galaxy backwards in time up to a maximum age of 80 Myr [2], as a function of the unknown radial velocity V_r. In agreement with Wex et al. (2000), we find that the system may have crossed the Galactic plane up to two times. The first Galactic plane crossing (case A) occurs at very young kinematic ages of $\simeq$ 2–4 Myr and gives rise to peculiar velocities in excess of $\simeq 300\,\mathrm{km\,s^{-1}}$. The corresponding post-SN orbital parameters are $A \approx 2.8\,R_\odot$ and $e \approx 0.618$. The second Galactic plane crossing (case B), on the other hand, takes place at least $\simeq 55$ Myr in the past and yields peculiar velocities of $\simeq$ 230–440 $\mathrm{km\,s^{-1}}$. The associated post-SN orbital separations and eccentricities range from $A = 3.1\,R_\odot$ and $e = 0.646$ to $A = 3.2\,R_\odot$ and $e = 0.658$.

The constraints on the pre-SN parameter space accessible to the progenitor of PSR B1913+16 are shown in Fig. 7 as functions of the unknown radial velocity V_r. As before, the red regions correspond to the solutions for which no mass transfer takes place at the time of the second SN explosion, while the blue regions indicate the additional solutions found when the possibility of mass transfer is taken into account. The constraints for detached pre-SN binary configurations are in good agreement with the constraints derived by Wex et al. (2000). It is clear however, that when the possibility of mass transfer is taken into account, the available parameter space becomes much less constrained.

[2] As for PSR J0737-3039 and PSR B1534+12, we use the spin-down age $\tau_b = 80$ Myr instead of the characteristic age $\tau_c = 110$ Myr as an upper limit for the age of the system. The maximum amount of orbital evolution that may have taken place since the formation of the DNS is therefore somewhat smaller than in Wex et al. (2000).

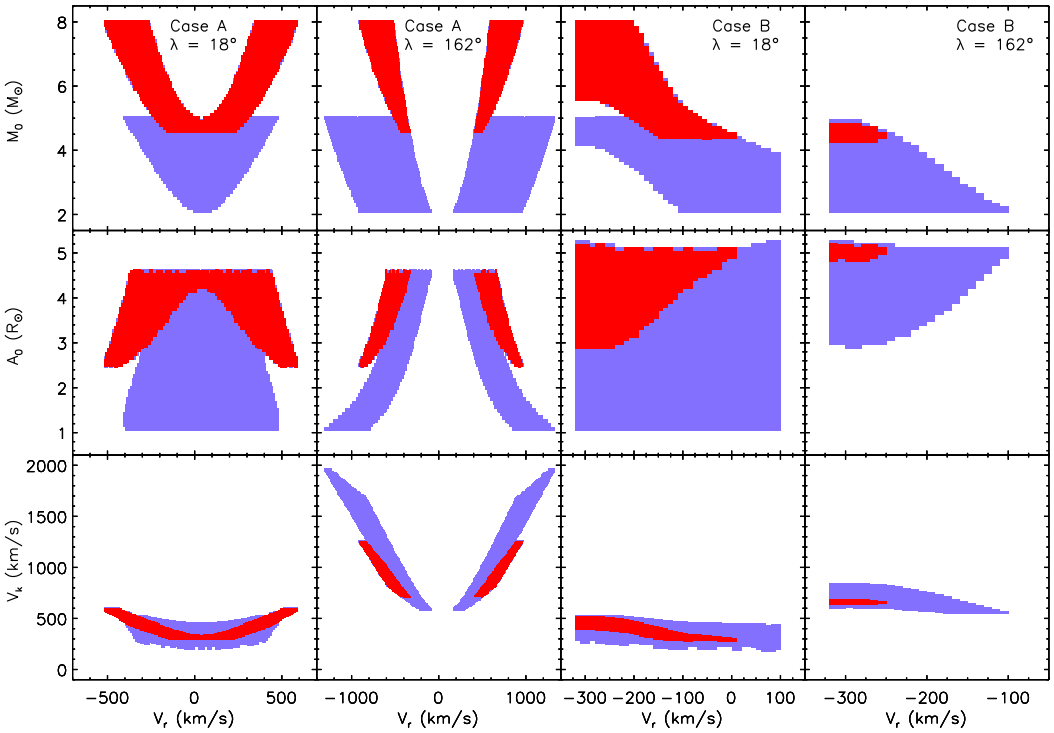

Fig. 7. Limits on the pre-SN progenitor of PSR B1913+16 and on the kick velocity imparted to the last-born NS. Red regions correspond to solutions for which the pre-SN binary is detached, while blue regions indicate the additional solutions associated with mass-transferring systems.

For case A disk crossings, the range of radial velocities for which physically acceptable solutions exist is restricted to $|V_r| \lesssim 500$–$600\,\mathrm{km\,s^{-1}}$ when $\lambda = 18°$, and to $100\,\mathrm{km\,s^{-1}} \lesssim |V_r| \lesssim 1300\,\mathrm{km\,s^{-1}}$ when $\lambda = 162°$. The mass of the second-born NS's direct progenitor is constrained to the interval between $2.1\,M_\odot$ and $8\,M_\odot$, and the pre-SN orbital separation to the interval between $1.1\,R_\odot$ and $5.3\,R_\odot$ for both considered values of the tilt angle λ. The magnitude of the kick velocity varies from $\simeq 190\,\mathrm{km\,s^{-1}}$ to $\simeq 600\,\mathrm{km\,s^{-1}}$ when $\lambda = 18°$ and from $\simeq 580\,\mathrm{km\,s^{-1}}$ to $\simeq 2000\,\mathrm{km\,s^{-1}}$ when $\lambda = 162°$. When the solutions are restricted to detached pre-SN binary configurations the limits become $300\,\mathrm{km\,s^{-1}} \lesssim V_k \lesssim 600\,\mathrm{km\,s^{-1}}$ and $700\,\mathrm{km\,s^{-1}} \lesssim V_k \lesssim 1250\,\mathrm{km\,s^{-1}}$ for $\lambda = 18°$ and $\lambda = 162°$, respectively.

For case B disk crossings, the mass M_0 of the second-born NS's direct progenitor and the pre-SN orbital separation A_0 are constrained to the ranges of values given by $2.1\,M_\odot \lesssim M_0 \lesssim 8\,M_\odot$ and $1.1\,R_\odot \lesssim A_0 \lesssim 5.3\,R_\odot$ when $\lambda = 18°$, and to $2.1\,M_\odot \lesssim M_0 \lesssim 5\,M_\odot$ and $2.9\,R_\odot \lesssim A_0 \lesssim 5.3\,R_\odot$ when $\lambda = 162°$. The magnitude of the kick velocity varies between $\simeq 190\,\mathrm{km\,s^{-1}}$ and $\simeq 530\,\mathrm{km\,s^{-1}}$ when $\lambda = 18°$, and between $\simeq 550\,\mathrm{km\,s^{-1}}$ and $\simeq 850\,\mathrm{km\,s^{-1}}$ when $\lambda = 162°$. When the solutions are restricted to those where no Roche-lobe overflow occurs at the time of the helium star's SN explosion, the minimum kick velocity associated with $\lambda = 18°$ increases slightly to approximately $280\,\mathrm{km\,s^{-1}}$, while

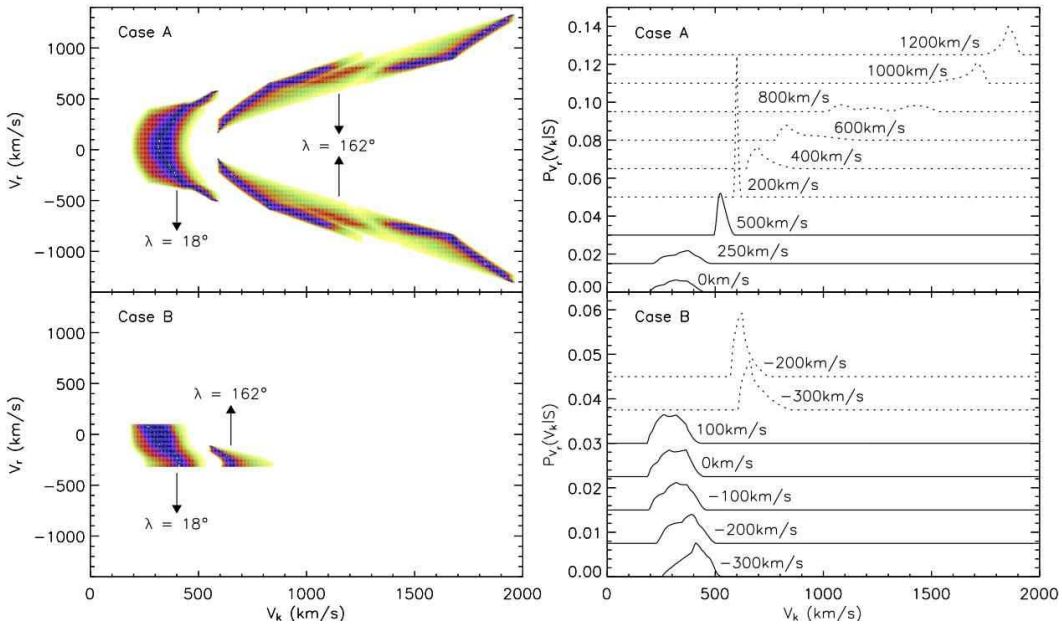

Fig. 8. Probability distribution functions of the magnitude of the kick velocity imparted to PSR B1913+16's companion at the time of its formation, for both $\lambda = 18°$ and $\lambda = 162°$ (cf. Fig. 5 for more details). In the right-hand panels, the solid lines correspond to $\lambda = 18°$ and the dashed lines to $\lambda = 162°$.

the range of admissible kick velocities associated with $\lambda = 162°$ becomes very tightly constrained to $V_k \approx 640$–$680\,\mathrm{km\,s^{-1}}$.

The probability distribution functions for the magnitude of the kick velocity imparted to the second-born NS in PSR B1913+16 are shown in Fig 8 for both $\lambda = 18°$ and $\lambda = 162°$. The distributions generally show a single peak at kick velocities which increase with increasing absolute values of V_r. For $\lambda = 18°$, the most probable kick velocity ranges from $\simeq 300\,\mathrm{km\,s^{-1}}$ to $\simeq 600\,\mathrm{km\,s^{-1}}$, while for $\lambda = 162°$ it ranges from $\simeq 600\,\mathrm{km\,s^{-1}}$ to almost $\simeq 2000\,\mathrm{km\,s^{-1}}$.

3 Formation Channels for Double Compact Objects

The inspiral and coalescence of double compact objects (DCO), such as NS-NS, BH-NS, and BH-BH binaries are some of the most promising candidate events for GW detection by current ground-based interferometers, like LIGO. The formation of double compact object populations has been studied by a number of different groups using population synthesis techniques. In one of these studies (Belczynski et al. 2002b) we focused on an investigation of the main formation channels, their origin, and their relative contributions. The details of this study the synthesis code used (*StarTrack*) and the conclusions are presented in Belczynski et al. (2002b). Here we merely summarize the findings

related to the various formation channels and their relative importance. Results are described for our standard model from that study (model A described in § 2.1 and § 2.2 of Belczynski et al. 2002b).

We consider double compact objects with NS or BH (NS-NS, BH-NS or BH-BH binaries) with merger times shorter than 10^{10} yr. In our standard evolutionary model, the population of coalescing DCO is dominated by NS-NS systems (61%), with a significant contribution by BH-BH binaries (30%), and a small contribution by BH-NS objects (9%).

In Table 3, we present the most important formation channels of coalescing DCO, for our standard model. Formation channels of NS-NS, BH-NS and BH-BH binaries are marked by NSNS, BHNS and BHBH, respectively, they are listed in order of decreasing relative formation frequency (second column) with respect to the whole DCO coalescing population. The details of each evolutionary sequence, i.e., MT episodes and SN explosions are also given. Results were obtained based on the evolution of 3×10^7 primordial binaries.

3.1 Populations of Double Neutron Stars

Belczynski et al. (2002b) identified a number of new NS-NS formation channels. This is a result of two improvements in the implementation of our population synthesis code, since Belczyński & Kalogera 2001, hereafter BK01. First, we have replaced the approximate prescription suggested by Bethe & Brown (1998) for the hyper-critical accretion during CE phases, with a newly derived numerical solution (see Appendix of Belczynski et al. 2002b). Second, we allow for hyper-critical CE evolution of low-mass helium stars with compact objects. In BK01, we allowed binaries with low-mass helium giants to evolve through DCE and standard SCE, but we had assumed that CE events of helium giants with compact objects lead to mergers, and possibly a gamma-ray burst (e.g., Fryer et al. 1998). However, due to the small mass of helium giant envelope at the onset of CE event ($\sim 1 - 1.5 M_{\odot}$), we find that these systems survive the CE events, and form very tight NS-NS binaries.

Double neutron stars are formed in various ways through more than 14 different evolutionary channels identified in Table 3. The relative formation efficiencies shown for each channel are for the standard model A, described in Belczynski et al. (2002b). The entire population of coalescing NS-NS systems, may be divided into three main subgroups.

Group I. This subpopulation consists of non-recycled NS-NS systems, first identified by BK01. These are systems in which none of the two NS ever had a chance of getting recycled through accretion. Our current results for the predicted formation rates and properties of the non-recycled NS-NS systems,

have not been affected by the two improvements discussed above. As shown

Double Compact Object Formation Channels

Formation Channel	Relative Efficiency[α]	Evolutionary History[β]
NSNS:01	20.3 %	NC:a→b, SN:a, HCE:b→a, HCE:b→a, SN:b
NSNS:02	10.8 %	NC:a→b, SCE:b→a, NC:a→b, SN:a, HCE:b→a, SN:b
NSNS:03	5.5 %	SCE:a→b, SN:a, HCE:b→a, HCE:b→a, SN:b
NSNS:04	4.0 %	NC:a→b, SCE:b→a, SCE:b→a, SN:b, HCE:a→b, SN:a
NSNS:05	3.2 %	DCE:a→b, SCE:a→b, SN:a, HCE:b→a, SN:b
NSNS:06	2.5 %	SCE:a→b, SCE:b→a, NC:a→b, SN:a, HCE:b→a, SN:b
NSNS:07	2.2 %	NC:a→b, NC:a→b, SN:a, HCE:b→a, HCE:b→a, SN:b
NSNS:08	2.0 %	NC:a→b, DCE:b→a, SN:a, HCE:b→a, SN:b
NSNS:09	2.0 %	DCE:a→b, DCE:a→b, SN:a, SN:b
NSNS:10	1.6 %	NC:a→b, SCE:b→a, SN:b, HCE:a→b, SN:a
NSNS:11	1.5 %	NC:a→b, SCE:b→a, DCE:b→a, SN:a, SN:b
NSNS:12	1.5 %	NC:a→b, SCE:b→a, DCE:a→b, SN:a, SN:b
NSNS:13	1.0 %	DCE:a→b, SN:a, HCE:b→a, SN:b
NSNS:14	3.0 %	all other
BHNS:01	4.5 %	NC:a→b, SN:a, HCE:b→a, SN:b
BHNS:02	1.6 %	NC:a→b, SCE:b→a, SN:a, SN:b
BHNS:03	1.3 %	SCE:a→b, SN:a, HCE:b→a, NC:b→a, SN:b
BHNS:04	2.0 %	all other
BHBH:01	17.7 %	NC:a→b, SN:a, HCE:b→a, SN:b
BHBH:02	10.5 %	NC:a→b, SCE:b→a, SN:a, SN:b
BHBH:03	1.4 %	all other

[α]Normalized to the total DCO population.

[β]Sequences of different evolutionary phases for the primary (a) and the secondary (b): non-conservative MT (NC), single common envelope (SCE), double common envelope (DCE), common envelope with hyper-critical accretion (HCE), supernova

explosion/core-collapse event (SN). Arrows mark direction of MT episodes.

in Table 3, the non-recycled NS-NS systems are formed via the NSNS:09, NSNS:11 and NSNS:12 channels, which involve DCE of two low-mass helium giants that were already allowed in the earlier version of *StarTrack*.

The unique qualitative characteristic of this NS-NS formation path is that both NS have avoided recycling. The NS progenitors have lost both their hydrogen and helium envelopes prior to the two supernovae, so no accretion from winds or Roche-lobe overflow is possible after NS formation. Consequently, these systems are detectable as radio pulsars only for a time ($\sim 10^6$ yr) much shorter than recycled NS-NS pulsar lifetimes ($\sim 10^8 - 10^{10}$ yr in the observed sample). Such short lifetimes are of course consistent with the number of NS-NS binaries detected so far and the absence of any *non-recycled* pulsars among them.

We note that the identification of the formation path for non-recycled NS-NS binaries stems entirely from accounting for the evolution of helium stars and for the possibility of double CE phases, both of which have typically been ignored in previous calculations (with the exception of Fryer et al. 1998, where, however, such events were assumed to lead to mergers).

Group II. This subpopulation consists of tight, short lived binaries with one recycled pulsar. Their merger times are typically ~ 1 Myr or even smaller (see § 3.4.5). As shown in Table 3, these new dominant NS-NS systems are formed via the NSNS:01–08, NSNS:10 and NSNS:13 channels, with the common characteristic that the *last* binary interaction is a hyper-critical CE of a low-mass helium giant and the first-born NS.

In Belczynski et al. (2002a) we describe in detail the formation of a typical NS-NS binary of group II. The channel identified as the most efficient for NS-NS formation (NSNS:01) corresponds to the "standard" channel of Fryer et al. (1998). The only difference is an extra CE event which originates from allowing for helium star evolution and without a priori assumptions about the CE outcome. The second most dominant channel, involving two consecutive MT episodes and then two SN explosions, closely resembles our channels: NSNS:02, NSNS:04, NSNS:06, NSNS:10, NSNS:11, NSNS:12. The only difference again remains an extra MT episode from evolved, Roche-lobe-filling helium stars.

The most dramatic effect of the binary evolution updates is reflected in the existence of a whole new population of coalescing NS-NS stars formed in Group II. In our standard model these channels contribute 50% of the DCO population, and their common characteristic is that the *last* binary interaction is a hyper-critical CE of a low-mass helium giant and the first-born NS [3]. It turns

[3] A more careful treatment of the response of helium stars to mass loss leads to a small reduction of this percentage, but the population forming through this channel

out that the majority of these systems survive the HCE event and form tight NS-NS binaries. Had we not taken into account the radial expansion of low-mass helium-rich giants, the progenitors of this dominant NS-NS population would have evolved without any further MT. Most of them would have still formed NS-NS systems, although not as tight as after this last CE episode. We have actually examined this alternative and found that about half of them would have formed binaries with merger lifetimes longer than 10^{10} yr.

Group III. This subpopulation consists of all the other NS-NS systems formed, through more or less classical channels (Bhattacharya & van den Heuvel 1991). The formation path denoted NSNS:14 corresponds to what is usually considered to be the "standard" NS-NS formation channel (Bhattacharya & van den Heuvel 1991). Since we account for hyper-critical accretion in CE, the formation rate is decreased because some NS (but not all, as assumed by Portegies Zwart & Yungelson 1998 and by Fryer et al. 1998) collapse to BH. Furthermore our treatment of the hyper-critical accretion typically leads to tighter post-CE systems, causing more binaries to merge in CE events, and thus decreases the number of possible NS-NS progenitors.

Brown (1995) proposed a NS-NS formation channel where the progenitor consists of two massive stars with nearly equal masses (within 4%) and the first mass transfer episode occurs when both stars are on the giant branch and have convective envelopes; if the binary survives the ensuing common envelope phase, both envelopes are ejected (double common envelope; DCE) and two helium stars are exposed which explode as supernovae and a NS-NS is formed. Brown was motivated by the almost equal mass measurements in NS-NS binaries and by adopting a low maximum NS mass ($1.5\,M_\odot$; associated with soft equations of state). In the proposed channel the progenitors are of almost equal mass and none of the NS ever experiences a common envelope phase, avoids collapsing into a BH. Some of the channels identified by Belczynski et al. (2002b) (Table 3; specifically NSNS:09,11,12) are similar to the Brown (1995) channel. However for the standard model they contribute only 8% of the total NS-NS population because a more widely accepted maximum neutron star mass of $3\,M_\odot$ is adopted and NS do not collapse into BH even if they experience hypercritical accretion in common envelopes (HCE). Recently Pinsonneault & Stanek (2006) reported on a population of "twin" binaries with component masses within 5%; this population about 50% of the observed sample, but of course it is also favored by selection effects and the true contribution of "twins" could be closer to 25% instead of 50%. Belczynski et al. (2002b) did also consider a model with a maximum NS mass of $1.5\,M_\odot$ (model D2); as expected the NS-NS rate is decreased significantly especially in comparison to BH-NS, since most of the standard NS-NS channels in Table 3 actually form BH-NS (the rate ratio shifts from 6.5 for the standard model A

is still significant, as discussed in Ivanova et al. (2003) and Belczynski et al. (2006a)

to 0.25 for model D2; see Table 4 in Belczynski et al. 2002b). We note that a more recent population study of the Brown (1995) channel presented by Dewi et al. (2006) leads to NS-NS rates consistent with that from model D2.

3.2 Populations of Black Hole Binaries

In general, BH-NS and BH-BH binaries are formed through just a few distinct channels, with a moderate number of MT events (2–3), in contrast to our findings for NS-NS systems. Helium star evolution, radial expansion and CE phases are much less important for their formation. The reason is that for most of these progenitors the first-born compact object is massive enough that they do not expand to large radii nor they lead to possible CE evolution (see channel BHNS:03 in Table 3). Instead these DCO form most efficiently through channels that closely resemble those NS-NS conventionally thought to be "standard" (Bhattacharya & van den Heuvel 1991; Fryer et al. 1998): evolution is initiated with a phase of non-conservative mass transfer and followed either by a CE phase or the formation of the first compact object (see BHNS:01, BHNS:02, and BHBH:01, BHBH:02).

4 Merger Rates of Double Neutron Stars: Observed Pulsar Sample

4.1 Introduction

Double Neutron Stars that will merge within a Hubble time are one of the prime targets for ground-based gravitational-wave (GW) interferometers such as GEO600, TAMA, VIRGO, and LIGO. Event rates of the DNS inspiral searches by these detectors can be inferred using the rate estimates with an extrapolation out to the maximum detection distances for any detector under consideration. Before 2003, the Galactic DNS merger rate had been estimated between $\sim 10^{-7} - 10^{-5}$ yr^{-1} (see Kalogera et al. 2001 and references therein). At that time, there were only two systems available for empirical studies, PSRs B1913+16 (Hulse & Taylor 1975) and B1534+12 (Wolszczan 1991). We calculated the PDF of Galactic DNS merger rates, $P(R)$, based on these two systems (see Kim et al. 2003, hereafter KKL, for further discussion [4]). Soon after the discovery of the highly relativistic system PSR J0737−3039 , we were able to revise $P(R)$ including PSR J0737−3039 in collaboration with the ob-

[4] We note that a web interface that allows the calculation of $P(R)$ for a wide range of pulsar surveys and pulsars is publicly available at http://www.astro.northwestern.edu/∼ciel/gppg_main.html

servation team [5] (Burgay et al. 2003; Kalogera et al. 2004a). The discovery of J0737−3039, resulted in a significant increase in the estimated Galactic DNS merger rate by a factor of ∼6. This implies a boost in event rates for DNS searches for GW interferometers. Here, we present our recent results on: (i) the PDF of Galactic DNS merger rate estimates with updated observations; (ii) the *global* PDF of rate estimates considering the systematic uncertainties; (iii) constraints on upper limits for rate estimates based on the observed supernova rate incorporated with our theoretical understanding of the SN-DNS relation; (iv) the approximate contribution of J1756−2251 to the Galactic DNS merger rates and uncertainties in our assumptions on the efficiency of the acceleration searches for Parkes multibeam pulsar survey (PMPS). Finally, we discuss implications of the most recently discovered pulsar binary J1906+0746 (Lorimer et al. 2006).

4.2 The Galactic DNS merger rate

Here, we describe the main components of the calculation of the combined $P(R)$ considering the three observed DNS systems in the Galactic disk. The details of these calculations are discussed by KKL and (Kalogera et al. 2004a). The merger rate of a given population i can be defined by

$$R_i \equiv \left(\frac{N_{\rm PSR}}{\tau_{\rm life}} f_{\rm b}\right)_i \ , \tag{3}$$

where $N_{\rm PSR,i}$ represents the number of pulsars in our Galaxy with pulse and orbital characteristics *similar* to an observed sample i (e.g. PSR J0739−3039) and $f_{\rm b,i}$ is a correction factor to take into account pulsar beaming (typically ~ 6) [6]; $\tau_{\rm life,i}$ is the lifetime of system i based on its observed properties. In order to calculate $N_{\rm PSR,i}$, we distribute a large population of pulsars *all* similar to the system i, in a model galaxy assuming spatial and luminosity distributions. Since pulsar luminosities are drawn from a distribution, the observed flux and estimated distance for the DNS system are not relevant in our calculation. Moreover, the selection effects for faint pulsars are implicitly taken into account. Once we generate a pulsar population with a size $N_{\rm PSR}$, we can then calculate the number of pulsars detected ($N_{\rm det}$) by large-scale pulsar surveys. We repeat the survey simulations with a detailed modeling of selection effects for observed DNS systems. For a fixed $N_{\rm PSR}$, we find that $N_{\rm det}$ follows a Poisson distribution, $\mathrm{P}(N_{\rm det}; \bar{N}_{\rm det})$, where $\bar{N}_{\rm det}$ is a mean value of $N_{\rm det}$ for a given population size ($N_{\rm PSR}$). We require $N_{\rm det} = 1$, i.e., we consider only one

[5] Only the millisecond component (J0737-3039A) is considered in our calculation. For instance, the current age of the system is derived from pulsar A.

[6] This is based on polarimetry measurements of B1913+16 and B1534+12.

observed system, and calculate the best-fit value of $\bar{N}_{\rm det}$. With a wide range of $N_{\rm PSR}$, we find $\bar{N}_{\rm det} = cN_{\rm PSR}$ as expected where c is a constant. Applying Bayes' theorem to these results, we calculate a P($N_{\rm PSR}$), a PDF for the population size of a given system i knowing that there is one observation. The calculation $P(R)$ from $P(N_{\rm PSR})$ is straightforwad, and the full derivation and the analytical formula can be found in Appendix A of Kim et al. (2004).

The lifetime of a DNS system is defined by $\tau_{\rm life} \equiv \tau_{\rm sd} + \tau_{\rm mrg}$, where $\tau_{\rm sd}$ is the spin-down age of a recycled pulsar (Arzoumanian et al. 1999) and $\tau_{\rm mrg}$ is the remaining lifetime until the two neutron stars merge (Peters & Mathews 1963). Based on the most recent observations, we estimate the lifetime of J0737−3039 to be ∼230 Myr (Lyne et al. 2004). This is the shortest among the three observed systems. The beaming correction factor $f_{\rm b}$ is defined as the inverse of the fractional solid angle subtended by the pulsar beam. Its calculation requires detailed geometrical information on the beam. Following Kalogera et al. (2001) and updating the values with recent observations, we calcualte $f_{\rm b}$∼5.7 for PSR B1913+16 (Weisberg & Taylor 2002) and ∼6.0 for PSR B1534+12 (Stairs et al. 2004) Without good knowledge of the geometry of J0737−3039, we assume $f_{\rm b,J0737}$ to be the average value of the other two systems ($\simeq 5.9$).

In Fig. 9, we show $P(R)$ for a reference model (Model 6 in KKL). We obtain the most likely value of $R \sim 71\,{\rm Myr}^{-1}$, larger by a factor of $\simeq 5.5$ than the rate estimated before the discovery of J0737−3039. The increase factor is found similar for all pulsar population models we examined. The increased merger rates imply a boost in the inferred detection rate of GWs from DNS inspirals for ground-based GW interferometers such as LIGO. In order to calculate the detection rate (D), we assume a homogeneous distribution of galaxies in nearby Universe and a spherical symmetry in detector sensitivity. Then, we can write D $\equiv R_{\rm gal} \times N_{\rm gal}$, where $N_{\rm gal}$ is the number of galaxies in the detection volumne ($V_{\rm det}$). We calculate the number density of galaxies derived by the observed blue luminosity density, ($n_{\rm gal} = 1.25\times10^{-2}{\rm Myr}^{-1}$ (see Phinney (1991) and Kalogera et al. (2001) for more details). The detection volume of LIGO can then be defined as a sphere for a given detection distance (20 Mpc and 350 Mpc for the inital and advanced LIGO, respectively), and the number of galaxies within $V_{\rm det}$ is simply $n_{\rm gal} \times V_{\rm det}$. For our reference model, we find that the most probable event rates are about 1 per 30 yrs and 1 per 2 days, for initial and advanced LIGO, respectively. At the 95% confidence interval, the most optimistic predictions for the reference model are 1 event per 9 yrs and 1.6 events per day for initial and advanced LIGO, respectively. More details can be found in Kalogera et al. (2004a).

As shown in Fig. 9, the Galactic DNS merger rate is dominated by PSR J0737−3039. We note that the current age of 30-70Myr for J0737−3039, suggested by Lorimer et al. (2005), implies a even shorter lifetime ($\tau_{\rm life} \sim 115-155$

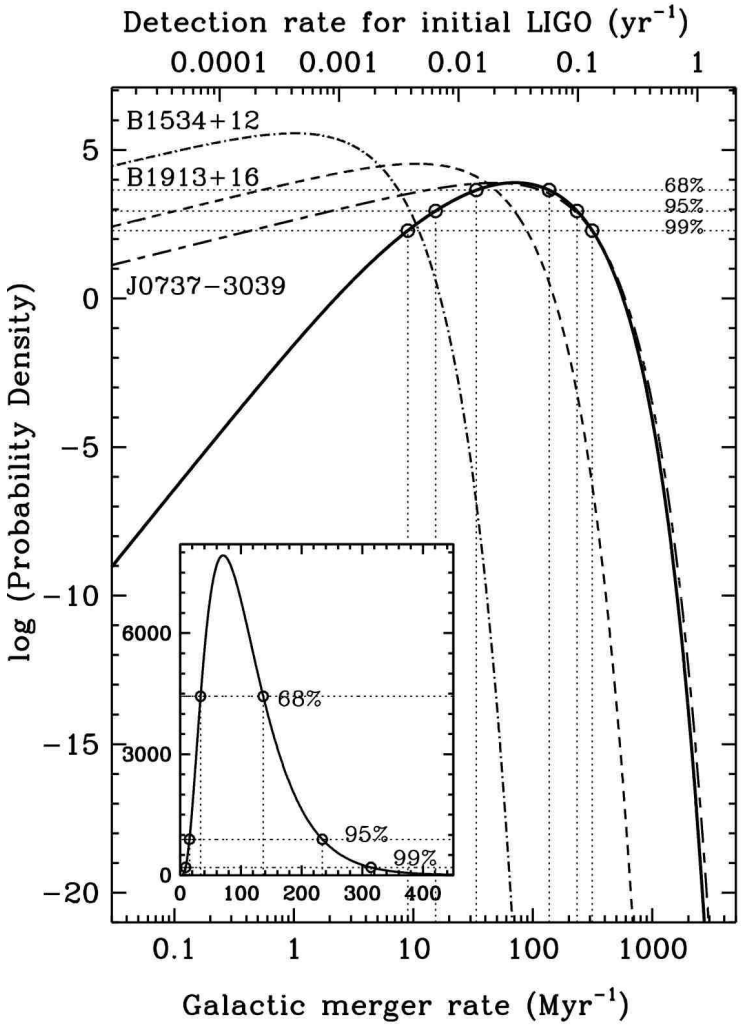

Fig. 9. $P(R)$ is shown on a log scale. The thick solid line is the Galactic rate estimate overlapped with results for individual observed systems (dashed lines). Dotted lines indicate confidence intervals for the rate estimates. The same results are shown on a linear scale in the small inset. All results are from our reference model.

Myr) knowing that the estimated merger timescale of this system is ∼85 Myr. Based on their results, we find the most likely value of R for the reference model is $\simeq 90 - 110\,\mathrm{Myr}^{-1}$.

The beaming correction for J0737−3039 is not yet constrained and we assume MSPs discovered in DNS systems are not very different. As a conservative lower limit, without any beaming corrections for all observed systems for a reference model, we obtain $\sim 12^{+11}_{-6}$ Myr^{-1} with a 95% confidence interval. The corresponding detection rates for initial and advanced LIGO are $5^{+12}_{-4} \times 10^{-3}$ yr^{-1} and 27^{+62}_{-21} yr^{-1}, respectively. Only when the axes geometry of J0737-3039 becomes available, we will be able to constrain the uncertainties of the beaming fraction, and in turn, the rate estimates.

4.3 Global probability distribution of the rate estimates

In KKL, we showed that empirical DNS merger rates are strongly dependent on the assumed luminosity distribution function for pulsars, but not on the pulsar spatial distribution. Therefore, we can consider only the rate dependence on the pulsar luminosity function for simplicity. Here, we describe how we can incorporate the systematic uncertainties from these models and calculate, $P_{\rm g}(R)$, a *global* PDF of rate estimates. Note that the results available on prior functions for pulsar luminosity distribution are currently out of date. Specific quantitative results could change when constraints on the luminosity function are derived from the current pulsar sample.

We assume a power-law luminosity distribution for a radio pulsar luminosity function $f(L)$. This function is defined by two parameters: the cut-off luminosity $L_{\rm min}$ and power-index p. We assume prior distributions for these two parameters and calculate $P_{\rm g}(R)$. We fit the marginalised likelihood of $L_{\rm min}$ and p presented by Cordes & Chernoff (1997) and obtain the following analytic formulae for prior functions, i.e. $f(L_{\rm min})$ and $g(p)$: $f(L_{\rm min}) = \alpha_0 + \alpha_1 L_{\rm min} + \alpha_2 L_{\rm min}^2$ and $g(p) = 10^{\beta_0 + \beta_1 p + \beta_2 p^2}$, where $\alpha_{\rm i}$ and $\beta_{\rm i}$ (i $= 0, 1, 2$) are coefficients we obtain from the least-square fits and the functions are defined over the intervals $L_{\rm min} = [0.0, 1.7]$ mJy kpc^2 and $p = [1.4, 2.6]$. We note that, although Cordes & Chernoff (1997) obtained $f(L_{\rm min})$ over $L_{\rm min} \simeq [0.3, 2]$ mJy kpc^2 centered at 1.1 mJy kpc^2, we consider $f(L_{\rm min})$ with a peak at ~ 0.8 mJy kpc^2 considering the discoveries of faint pulsars with $\rm L_{1400}$ below 1 mJy kpc^2 (Camilo 2003). Next we calculate $P_{\rm g}(R)$ as follows:

$$P_{\rm g}(R) = \int_p dp \int_{L_{\rm min}} dL_{\rm min} P(R) f(L_{\rm min}) g(p). \quad (4)$$

In Fig. 10, we show the distributions of $L_{\rm min}$ and p adopted (top panels) and the resulting global distribution of Galactic DNS merger rate estimates (bottom panel). We find the peak value of $P_{\rm g}(R)$ at *only* around 13 Myr^{-1}. We note that this is a factor ~ 5.5 smaller than the result from our reference model ($R \sim$71 Myr^{-1}). At the 95% confidence interval, we find that the *global* Galactic DNS merger rates lie in the range $\sim$ 1–145 Myr^{-1}. These imply LIGO event rates in the range $\sim (0.4 - 60) \times 10^{-3}$ yr^{-1} (initial) and $\sim 2 - 330$ yr^{-1} (advanced). Since 1997, the number of known millisecond pulsars has more than doubled, and therefore, constraints on $L_{\rm min}$ and p and their PDFs based on the most up-to-date pulsar sample are urgently needed.

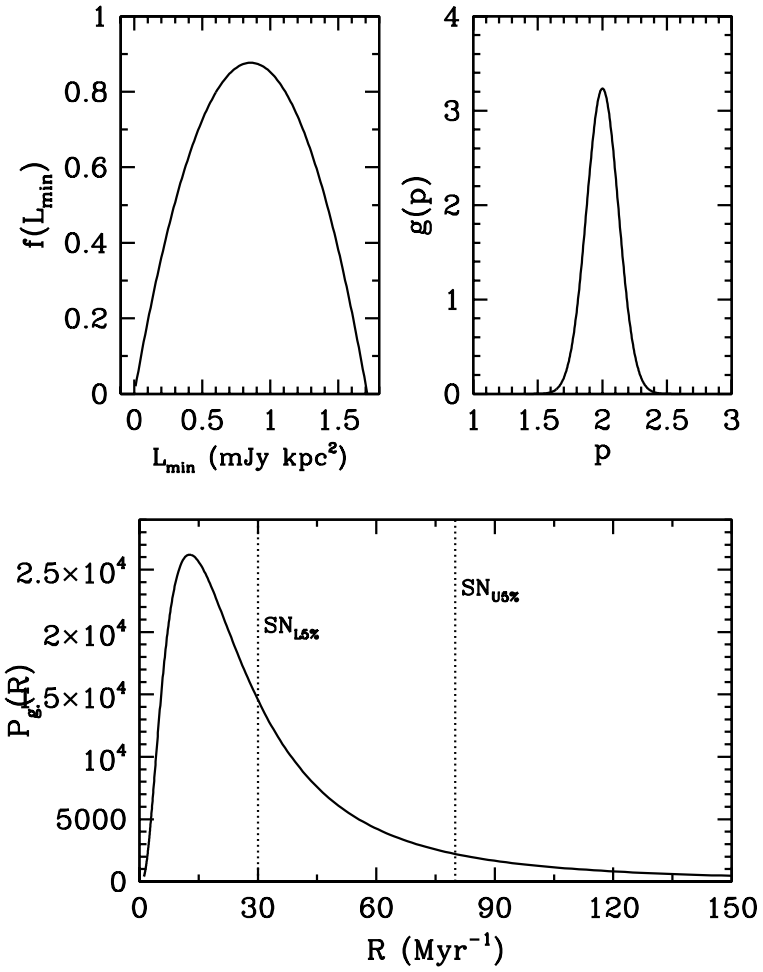

Fig. 10. The global $P_{\rm g}(R)$ on a linear scale (lower panel) and the assumed intrinsic distributions for $L_{\rm min}$ and p (upper panels). Dotted lines represent the lower ($SN_{\rm L}$) and upper ($SN_{\rm U}$) bounds on the observed SN Ib/c rate scaled by 5% of the observed SN Ib/c rates, $600 - 1600$ Myr^{-1} (see text).

4.4 Upper Limit of DNS Merger Rate Estimates. Constraints from Type Ib/c Supernovae Rates

According to the standard binary evolution scenario, the progenitor of the second neutron star is expected to form during a Type Ib/c supernova. Therefore, the empirical estimates for the Type Ib/c SN rate in our Galaxy can be used to set upper limits on the DNS merger rate estimates. Based on Cappellaro et al. (1999), we adopt $R_{\rm SN\,Ib/c} \simeq 1100 \pm 500\,{\rm Myr}^{-1}$ considering Sbc–Sd galaxies, a Hubble constant $H_0 = 71\,{\rm km/s/Mpc}$ and the blue luminosity of our Galaxy $L_{\rm B,gal} = 9 \times 10^9\,L_{\rm sun}$.

We calculate the fraction of SN Ib/c actually involved in the formation of DNS with a binary evolution code *StarTrack* (Belczynski et al. 2002b, 2006b) and estimate the rate ratio: $\gamma \equiv (R_{\rm DNS}/R_{\rm SN\,Ib/c}) \times 100 \leq 5\%$. Motivated by this result, we adopt the empirical $R_{\rm SN\,Ib/c}$ assuming $\gamma \sim 5\%$ and compare the value with the global PDF (Fig. 10).

We note that our most optimistic DNS merger rate is $R = 189^{+691}_{-166}$ Myr^{-1} at a 95% confidence interval (Model 15 in KKL). We obtain $\gamma \sim 80\%$ with respect to the center value of the empirical SN Type Ib/c rate (1100 Myr^{-1}) and the upper limit of R at the 95% confidence interval ($189 + 691 = 880$ Myr^{-1}). This corresponds to $\gamma \sim 13\%$ for a SN Type II rate, which is factor 6.1 larger than that of SN Type Ib/c. In both cases, the most optimistic model is lower than the current empirical supernova rate estimates, but not really consistent with the results of population synthesis calculations. If we consider an upper limit of R at the 95% confidence interval from the global PDF, we obtain $\gamma \sim 13\%$ and 2% for the center value of SN Type Ib/c (1100 Myr^{-1}) and II, respectively.

4.5 Implications of New Discoveries to the Galactic DNS merger rate estimates

Recently, Faulkner et al. (2005) discovered PSR J1756−2251, the 4th merging DNS in the Galactic disk from the Parkes Multibeam Pulsar Survey (PMPS). The standard Fourier method failed to find this pulsar and they reanalysed the PMPS data with an acceleration search (or a 'stack search' as described in their paper). In order to calculate the merger rate including PSR J1756−2251, a detailed simulation is necessary to calculate the effect of the acceleration search with the PMPS. However, the approximate contribution of PSR J1756−2251 to the Galactic merger rate can be easily obtained. We find the total rate increases by only $\sim 4\%$ due to the new discovery. This is expected because PSR J1756−2251 can be identified as a member of the B1913+16-like population, which has already been taken into account in the calculation. Only future detections of pulsars from a significantly different population (compared to the known systems), or from the most relativistic systems, will result in a non-trivial contribution to the rate estimates.

Finally, we note the implications of J1906+0746 on the pulsar binary merger rates. This system has drawn attention due to the extremely young age of the pulsar (characteristic age of ~ 112 kyr; Lorimer et al. 2006). If the companion is another neutron star, J1906+0746 would be the first discovery of a non-recycled component in a DNS system. Currently, the nature of the companion is totally unknown, and it can be either a light neutron star, or heavy (O-Mg-Ne) white dwarf. Assuming J1906+0746 is a DNS system, we

calculate its contribution to the Galactic merger rate. Because of its short lifetime (∼82Myr), J1906+0746 can increase the Galactic DNS merger rate by about a factor 2. This implies that the current estimated DNS merger rate including J0737−3039 can still be doubled! If J1906+0746 is an eccentric NS–WD system, such as J1141-6545 (van Kerkwijk & Kulkarni 1999) or B2303+46 (Stokes et al. 1985), it will be as important as J1141-6545, which is currently dominate the birthrate of eccentric NS-WD binaries.

5 Merger Rates of Double Compact Objects: Population Synthesis

Lacking a sample of DCOs containing a black hole, the only route to BH-BH merger rates is via population synthesis models. These involve a Monte Carlo exploration of the likely life histories of binary stars, given statistics governing the initial conditions for binaries and a method for following the behavior of single and binary stars (see, e.g., Belczynski et al. 2002b; Hurley et al. 2002; Portegies Zwart & Verbunt 1996; Fryer et al. 1998, and references therein). Unfortunately, our understanding of the evolution of single and binary stars is incomplete, and we parameterize the associated uncertainties with a great many parameters (~ 30), many of which can cause the predicted DCO merger rates to vary by more than one or two orders of magnitude when varied independently through their plausible range. To arrive at more definitive answers for DCO merger rates, we must substantially reduce our uncertainty in the parameters that enter into population synthesis calculations through comparison with observations when possible.

The simplest and most direct way to constrain the parameters of a given population synthesis code is to compare several of its many predictions against observations. For example, O'Shaughnessy et al. (2005b) required their population synthesis models be consistent with the empirically estimated formation rates derived from the four known Galactic NS−NS binaries which are tight enough to merge through the emission of gravitational waves within 10 Gyr. Here, we require our population synthesis models to be consistent (modulo experimental error) with six observationally determined rates: (i) the formation rate implied by the known Galactic merging NS−NS binaries, mentioned above; (ii) the formation rate implied by the known Galactic NS−NS binaries which do *not* merge within 10 Gyr (henceforth denoted "wide" NS−NS binaries); (iii,iv) the formation rate implied by the sample of merging and eccentric WD-NS binaries; and finally (v,vi) the type II and type Ib/c SNe rates. Further, we use the set of models consistent with these constraints to revise our population-synthesis-based expectations for various DCO merger rates, assuming no prior information, so all population synthesis model parameters consistent with our constraints are treated equally.

5.1 Observations of DCOs

Seven NS−NS binaries and four WD-NS binaries (with relatively massive WDs) have been discovered so far in the galactic disk, using pulsar surveys with well-understood selection effects. [We are very specifically *not* including the recently-discovered binary PSR J1906+0746 (Lorimer et al. 2006), because the companion cannot be definitively classified as a WD or NS at present. We also omit PSR J2127+11C found in the globular cluster M15, since its formation is thought to be dynamical and not due to isolated binary evolution in the Galactic field.

5.2 Methodology I: Preferred population model

As already discussed, in the context of NS−NS KKL developed a statistical method to estimate the likelihood of DCO formation rates, given an observed sample of DCOs in which one member is a pulsar, designed to account for the small number of known systems and their associated uncertainties. In this section, we present results only for our reference pulsar luminosity distribution model, corresponding a power law luminosity distribution with negative slope, index $p = 2$, and minimum luminosity $L_{min} = 0.3$ mJy kpc^2 [model 6 of KKL; as discussed therein, this model better accounts for more recent observations of faint pulsars]; in the following section, we describe our our predictions change when systematic uncertainties in p and L_{min} are incorporated into $\mathcal{P}$.

Finally, for each class of binary pulsars we define symmetric 95% confidence intervals: the upper and lower rate limits $\mathcal{R}_{w,\pm}$ satisfy

$$\int_0^{\mathcal{R}_{w,-}} d\mathcal{R}\mathcal{P}_w(\mathcal{R}) = \int_{\mathcal{R}_{w,+}}^{\infty} d\mathcal{R}\mathcal{P}_w(\mathcal{R}) = 0.025 \; . \tag{5}$$

This confidence-interval convention is different from with the customary choice presented in KKL.

In all plots that follow, rate probability distributions are represented using a logarithmic scale for $\mathcal{R}$; thus, instead of plotting $\mathcal{P}$, all plots instead show

$$p(\log \mathcal{R}) = \mathcal{P}(\mathcal{R})\mathcal{R} \ln 10 \; .$$

5.2.1 WD-NS binaries

Four WD-NS binaries with relatively massive WDs have been discovered in the galactic disk: PSRs J0751+1807, J1757-5322, J1141-6545, and B2303+46. While all four binaries may be applied to a *net* WD-NS formation rate estimate, the sample manifestly contains relics of distinctly different evolutionary channels; for example, while J0751+1807 and J1757-5332 have evidently been strongly circularized and spun up by a recent mass transfer episode, J1141-6545 cannot have been (Kaspi et al. 2000; Bailes et al. 2003). Ideally, population synthesis must produce distributions of WD-NS binaries consistent with both the observed orbital parameters and spins; however, the present sparse sample does not allow a reliable nonparametric estimate of the distribution of WD-NS binary parameters. Instead, as first step towards applying constraints based on binary parameter *distributions*, we subdivide these five binaries into two overlapping classes: *merging* binaries, denoted WD-NS(m), which will merge through the emission of gravitational waves within 10 Gyr; and *eccentric* binaries, denoted WD-NS(e), which have significant ($e > 0.1$) eccentricity at present. The rate estimate derived for both classes is dominated by J1141-6545 (Kim et al. 2004; Kalogera et al. 2005).

5.2.2 NS−NS binaries

Seven NS−NS binaries have been discovered so far in the Galactic disk. Four of the known systems will have merged within 10 Gyr (i.e., "merging" binaries: PSRs J0737-3039, B1913+16, B1534+12, and J1756-2251) and three are wide with much longer merger times (PSRs J1811-1736, J1518+4904, and J1829+2456). PSR J1756-2251 was discovered recently with acceleration searches (Faulkner et al. 2005). As already discussed, the rate increase is estimated to be smaller than 4%. For this reason, we omit it when estimating NS-NS merger rates.

The observed NS-NS population naturally subdivides into two distinct classes, depending on whether they merge due to the emission of gravitational waves within 10 Gyr: *merging* NS−NS binaries, denoted NSNS(m), and *wide* NS−NS binaries, denoted NSNS(vw).

5.2.3 Recycling, selection effects, and the lack of wide NS-NS binaries

We find that the confidence intervals for wide and merging NS-NS binaries are almost an order of magnitude from overlapping. On the contrary, population synthesis simulations produce merging and wide binaries at a roughly equal (and always highly correlated) rates. Since our rate estimation technique automatically compensates for the most obvious selection effects (e.g., orientation and detectable lifetime), two unbiased samples of wide and merging NS-NS

binaries should arrive at nearly the *same* prediction for the NS-NS formation rate.

O'Shaughnessy et al. (2005b) explained this significant discrepancy by a selection effect: evolutionary tracks leading to wide NS-NS binaries should be less likely to recycle the first-born pulsar. The *observed* sample of wide NS-NS binaries [NSNS(vw)] represents a much smaller subset of *recycled* pulsars. As summarized in O'Shaughnessy et al. (2006a), we assume any wide NS-NS binary which in its past underwent *any conventional* mass transfer will recycle one of its neutron stars to a pulsar. This condition is likely to over-estimate the true NSNS(vw) formation rate. We note that neutron-star recycling can also possibly happen during dynamically unstable mass-transfer phases (common envelopes), but the vast majority of wide NS-NS do not evolve through such a phase.

5.2.4 Pulsar Population Model Uncertainties

As noted in KKL and subsequent papers, our reconstruction of the pulsar population (i.e., N_{PSR}) relies upon our understanding of pulsar survey selection effects and thus on the underlying pulsar luminosity distribution. This distribution can be well-constrained experimentally (see, e.g. Cordes & Chernoff 1997), though these constraints do not yet incorporate recent faint pulsar discoveries such as J1124-5916 (Camilo et al. 2002). Nonetheless, different observationally-consistent distributions imply significantly different distributions, with maximum-likelihood rates differing by factors of order 10 (Kim et al. 2003). Since the constraint intervals discussed above assume the *preferred pulsar luminosity distribution model* – a power-law pulsar luminosity distribution with negative slope $p = 2$ and minimum cutoff luminosity $L_{min} = 0.3$ mJy kpc^2 – they do not incorporate any uncertainty in the pulsar luminosity function.

The infrastructure needed to incorporate uncertainties in the pulsar luminosity function has been presented in § 4.2. However, out-of-date constraints on the pulsar luminosity function allow implausibly high minimum pulsar luminosities L_{min}. A high minimum pulsar luminosity implies fewer merging pulsars have been missed by surveys. Thus, these out-of-date constraints on pulsar luminosity functions permit models consistent with substantially lower merger rates than now seem likely, given the discovery of faint pulsars. In other words, if we use the infrastructure presented in Kim et al. (2006) to marginalize over L_{min} and p generate a *net* distribution function for the merger rate, then the 95% confidence intervals associated with that net distribution would have a spuriously small lower bound, entirely because the pulsar population model permits large L_{min}. Therefore, we present results based only on our preferred luminosity function and do not include the out-of-date luminosity function constraints by Cordes & Chernoff (1997) and the related net rate distribution

provided by Kim et al. (2006).

5.3 Observations of supernovae

Type Ib/c and II supernovae occur extremely rarely near the Milky Way. While historical data contains several observations of and even surveys for supernovae, the selection effects in these long-duration heterogeneous data sets have made their interpretation difficult (Cappellaro 2005, private communication). In this paper, we estimate supernova rates and uncertainties via Table 4 of Cappellaro et al. (1999). Cappellaro et al. (1999) present their results in terms of a number of supernovae per century per 10^{10} blue solar luminosities ($L_{\odot,B}$); to convert their results to rates per Milky Way equivalent galaxy, we assume a Milky Way blue luminosity of $2 \times 10^{10} L_{\odot,B} = 0.9 \times 10^{10} L_{\odot}$ relative to the solar blue ($L_{\odot,B}$) and total ($L_{\odot}$) luminosities (see, e.g., Kalogera et al. (2001), Phinney (1991), Cox (2000) and references therein). Using their estimates for the most-likely supernovae rates and for the 1σ errors in those rates for Milky Way-like galaxies (i.e., S0a-Sb), we arrive at the 2σ logarithmic confidence intervals used in our constraints.

Though fairly accurate studies exist of the high-redshift supernova rate (e.g., Cappellaro et al. 2005), they have little relevance to the present-day Milky Way. Several surveys have also attempted to determine the supernova rate in the Milky Way by a variety of indirect methods, such as statistics of supernova remnants (highly unreliable due to challenging selection effects; see, e.g., van den Bergh & Tammann 1991) and direct observation of radioisotope-produced backgrounds (e.g., decay from ^{26}Al, as described in Diehl et al. 2006). Taken independently, these methods have greater uncertainties than the historical studies of Cappellaro et al. (1999).

5.4 Population synthesis predictions

5.4.1 StarTrack *population synthesis code*

We estimate formation and merger rates for several classes of double compact objects using the *StarTrack* code first developed by Belczynski et al. (2002b) and recently significantly updated and tested as described in detail in Belczynski et al. (2006b). This updated code predicts somewhat different double compact object properties than the version used in Belczynski et al. (2002b); a forthcoming paper (Belczynski et al., in preparation) will discuss these changes and the evolutionary physics underlying them in significantly greater detail.

Like any population synthesis code, it evolves randomly chosen binaries from their birth to the present, tracking the stellar and binary parameters. For any class of events that is *identifiable within the code*, such as supernovae or DCO mergers, we estimate event rates by taking the average event rate within the simulation (i.e., by dividing the total number of events seen within some simulation by the duration of that simulation) and renormalizing by a scale factor that depends on properties of the simulation (i.e., the number of binaries simulated and the binary birth mass distributions assumed) and the Milky Way as a whole (i.e., the present-day star formation rate); see Eq. (2) and Appendix A of O'Shaughnessy et al. (2005a) for details. Specifically, our simulations [7] are normalized to be consistent with an assumed Milky Way star formation rate of $3.5 M_{\odot} \mathrm{yr}^{-1}$.

When constructing our archived population synthesis results, we did not choose to record detailed information about the nature and amount of any mass transfer onto the first-born NS. We therefore cannot reconstruct precise population synthesis predictions for the NSNS(vw) formation rate. However, we do record whether some mass transfer occurs, and the nature of the mass transfer mechanism. The conventional mass transfer mechanism – dynamically stable Roche-lobe overflow – inevitably produces a disk around the compact object and can potentially spin that object up. Other mechanisms, such as (possibly hypercritical) common-envelope evolution, presumably involve a substantially more spherical accretion flow; the specific angular momentum accreted may be substantially lower, possibly not enough to recycle the neutron star. Thus for the purposes of identifying a class of potentially recycled ("visible") wide NS-NS binaries, we assume any system which underwent mass transfer (dynamically stable in the case of wide systems) produced a recycled NS primary.

5.4.2 Fitting results

As in previous studies such as O'Shaughnessy et al. (2005a), here we have chosen to vary seven (7) model parameters in the synthesis calculations. These choices are strongly guided by our past experience with double-compact-object population synthesis and represent the model parameters for which strong dependence has been confirmed. These seven parameters enter into every aspect of our population synthesis model. One parameter, a power law index r in

[7] Our approach gives only the *average* event rate. The present-day merger rate agrees with this quantity when most mergers occur relatively promptly (e.g., < 100 Myr) after their birth. Some DCOs – notably double BH binaries – have substantial delays between birth and merger, introducing a strong time dependence to the merger rate. The technique described above will significantly *underestimate* these rates. This point will be addressed in considerably more detail, both for the Milky Way and for a heterogeneous galaxy population in a forthcoming paper by O'Shaughnessy et al. (2006a).

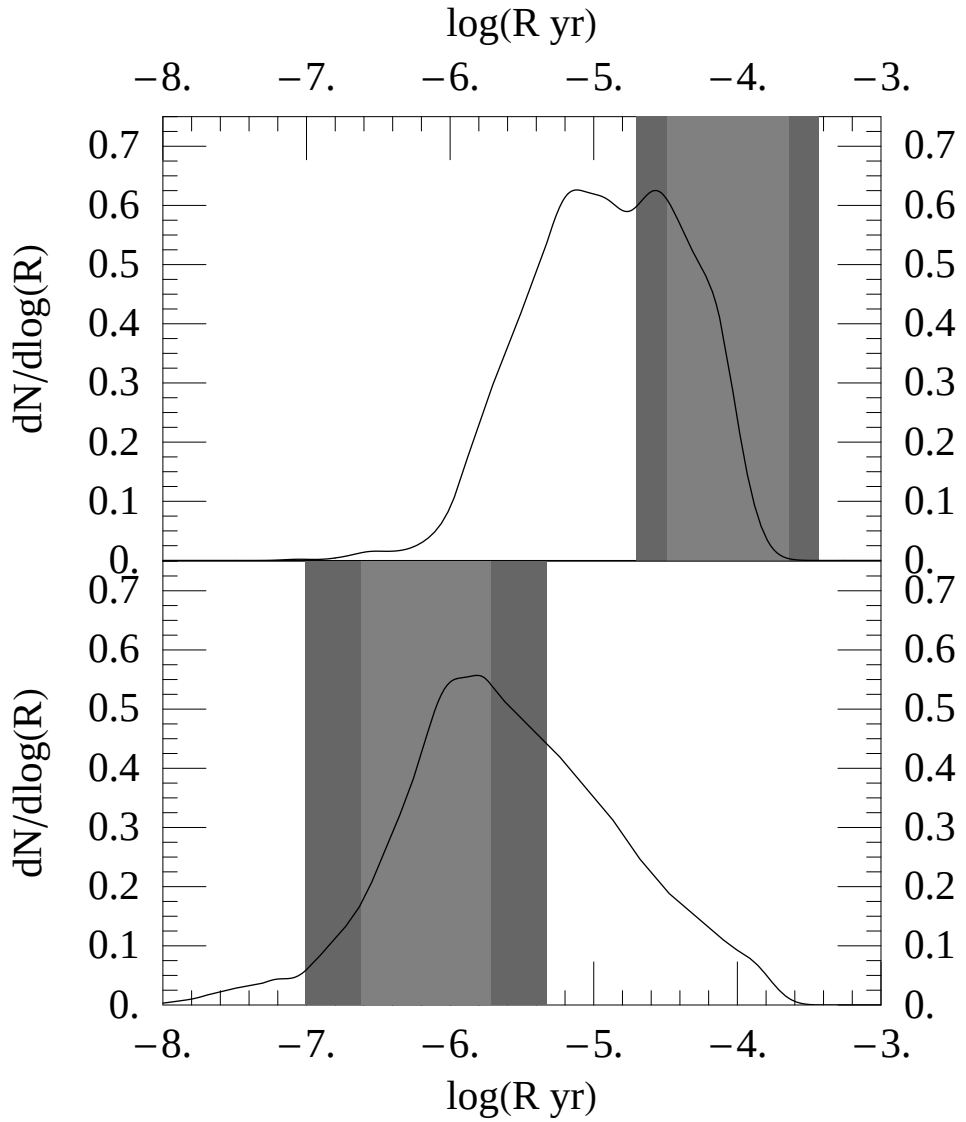

Fig. 11. Probability distributions for merging (top) and wide (bottom) NS-NS formation rates, as predicted by population synthesis. The light shaded region shows the 95% confidence interval consistent with observations of binary pulsars, as described in Sec. 5.1. Because of sparse sampling and relatively poor data, our fit for the formation rate of visible, wide NS-NS binaries is significantly more uncertain than other fits.

our parameterization of the companion mass distribution, influences the initial binary parameter distributions (through the companion masses). Another parameter w, the massive stellar wind strength, controls how rapidly the massive progenitors of compact objects lose mass; this parameter strongly affects the final compact-object mass distribution. Three parameters $v_{1,2}$ and s are used to parameterize the supernovae kick distribution as a superposition of two independent maxwellians. These kicks provide critical opportunities to

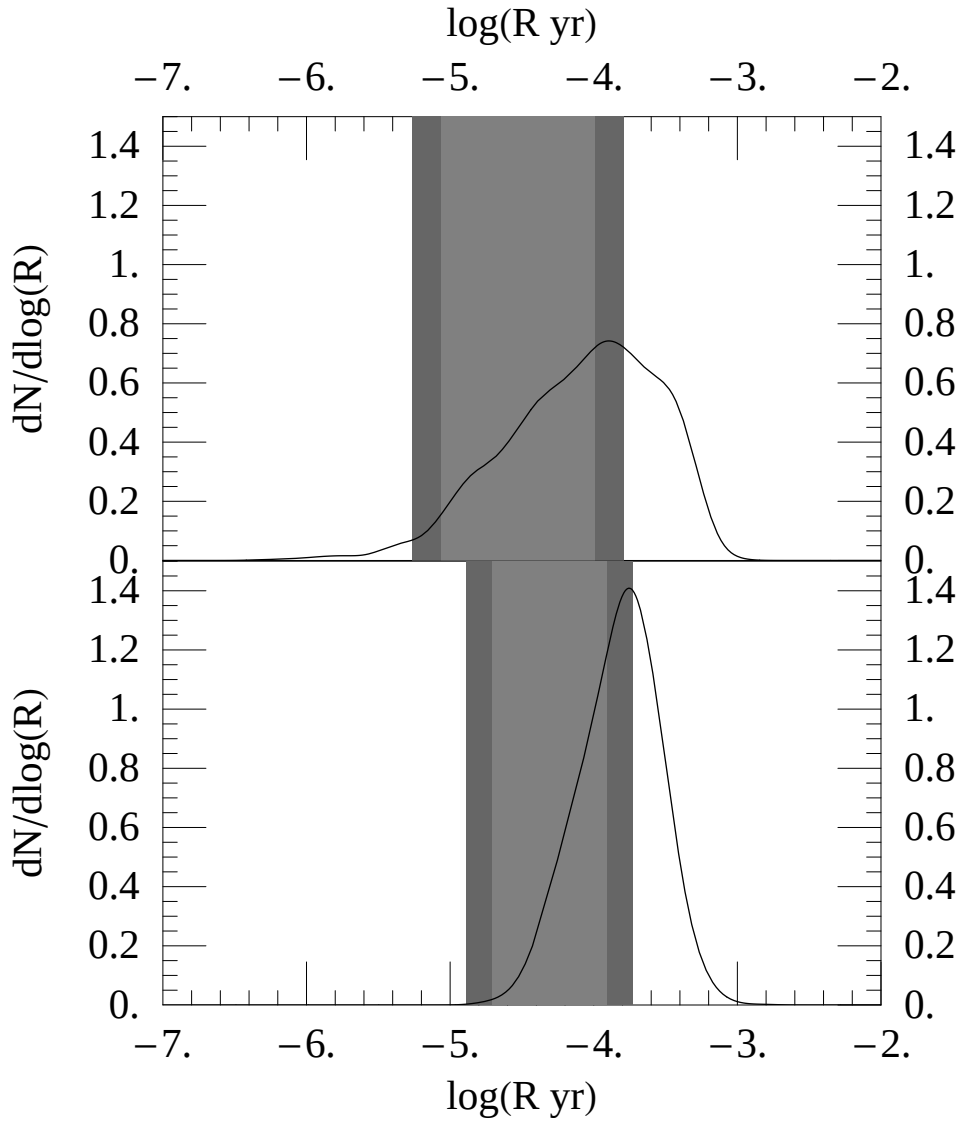

Fig. 12. Probability distributions for merging (top) and eccentric (bottom) WD-NS formation rates, as predicted by population synthesis. The light shaded region shows the 95% confidence interval consistent with observations of binary pulsars, as described in Sec. 5.1. The dark shaded region extends this constraint interval by an estimate of the systematic error in each fit; see O'Shaughnessy et al. (2006a).

push distant stars into tight orbits and also to disrupt potential double neutron star progenitors. Finally, two parameters $\alpha\lambda$ and f_a govern energy and mass transfer during certain types of binary interactions; see Section 2.2.4 of Belczynski et al. (2002b) for details. To allow for an extremely broad range of possible models, we consider the specific parameter ranges quoted in §2 of O'Shaughnessy et al. (2005a) for all parameters except kicks; for supernova kick parameters, we allow the dispersion $v_{1,2}$ of either component of a bimodal Maxwellian to run from 0 to 1000 km/s.

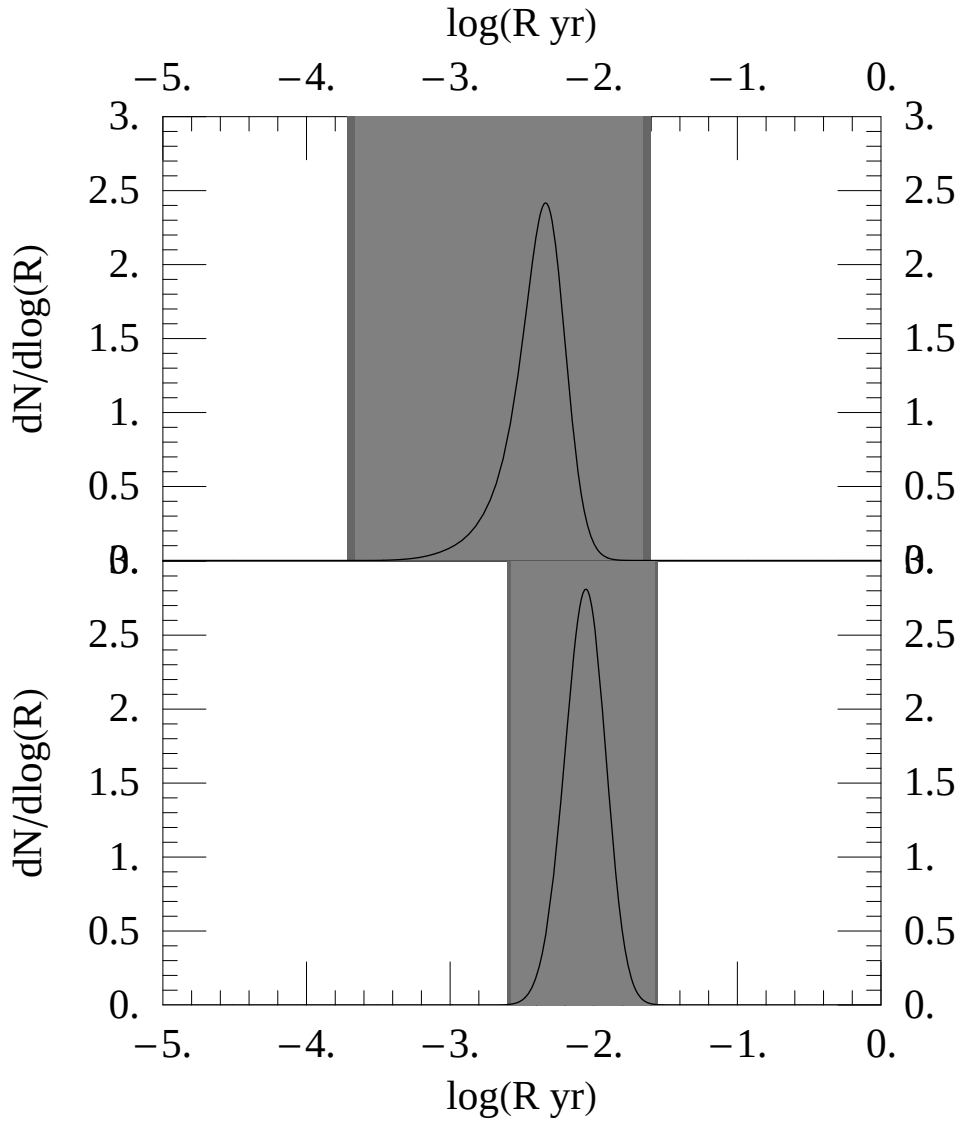

Fig. 13. Probability distributions for SN Ib/c (top) and SN II (bottom), as predicted by population syntheses with *StarTrack*. The light shaded region shows the ($\approx 2\sigma$) interval consistent with observational constraints of supernovae, from Cappellaro et al. (1999). A dark shaded region (not visible in this plot) indicates these constraints, augmented by an estimate of the systematic errors in our fits; see O'Shaughnessy et al. (2006a). These constraints provide no information about population synthesis.

Since population synthesis calculations involve considerable computational expense, in practice we estimate the merger rate we expect for a given combination of population synthesis model parameters via seven-dimensional fits to an archive of roughly 3000 detailed simulations, as presented and analyzed in detail in O'Shaughnessy et al. (2006a) (hereafter OKB). However, these fits introduce systematic errors, which have the potential to significantly change

the predicted set of constraint-satisfying models. For this reason, OKB also estimate the rms error associated with each seven-dimensional fit. Finally, OKB demonstrate that, by broadening the constraint-satisfying interval by the fit's rms error, the predicted set of constraint-satisfying models includes most models which *actually* satisfy the constraints. For this reason, the dark shaded regions in Figures 11, 12, and 13 account for both observational uncertainty in the Milky Way merger rate and for systematic errors in the fits against which these observations will be compared.

5.5 Prior distributions

Lacking knowledge about which population synthesis model is correct, we assume all population synthesis model parameters in our range are *equally likely*. A monte carlo over the seven-dimensional parameter space allows us then to estimate the relative likelihood, all things being equal, of various DCO merger rates (shown in Figures 11,12) and supernova rates (Figure 13). Also shown in these figures are the observational constraints described in Sections 5.2.1, 5.2.2 and 5.3 (shown in shaded gray). Finally, the dotted lines in Figure 15 show the a priori population synthesis predictions for BH-BH, BH-NS, and NS-NS merger rates in the Milky Way.

5.6 Applying and employing constraints

Physically consistent models must reproduce all predictions. Supernovae rates, being ill-determined due to the large observational systematic errors mentioned in Sec. 5.3, are easily reproduced by almost all models at the 2σ level; see Fig. 13. However, population synthesis models do not always reproduce observed formation rates for DCOs, as shown in Figs. 12 and 11. These four 95% confidence intervals implicitly define a $(0.95)^4 \approx 81\%$ confidence interval in the seven-dimensional space, consisting of 9% of the original parameter volume when systematic errors in our fitting procedure are included. In other words, we are quite confident (80% chance) that the physically-appropriate parameters entering into *StarTrack* can be confined within a small seven-dimensional volume, in principle significantly reducing our model uncertainty.

In Figure 14 we show one-dimensional projections onto each coordinate axis of the constraint-satisfying volume – in other words, the distribution of values each *individual* population synthesis parameter can take. For the purposes of this and subsequent plots, we use the following seven dimensionless parameters x_k that run from 0 to 1: $x_1 = a/3$; $x_2 = w$; $x_3 = v_1/(1000\text{km/s})$, $x_4 = v_2/(1000\text{km/s})$; $x_5 = s$; $x_6 = \alpha\lambda$, and $x_7 = f_a$. As seen in the top panel of this figure, the conditional distribution of supernovae kicks bears

a surprising resemblance to the observed pulsar kick distribution (see, e.g., Arzoumanian et al. 1999; Hobbs et al. 2005; Faucher-Giguere & Kaspi 2006, and references therein), even though *no information about pulsar motions have been included* among our constraints and priors. The population synthesis mass transfer parameter f_a is also well-constrained, with a strong maximum near $x = 0$, implying that mass-loss fractions of about 90% or higher are favored in non-conservative, but stable, mass transfer episodes. Also, common envelope efficiencies $\alpha\lambda$ of about 0.2-0.5 appear to be favored by the constraints. The rest of the one-dimensional parameter distributions are nearly constant and thus uninformative. Though small, the constraint-satisfying volume extends throughout the seven-dimensional parameter space.

Evaluating fits for other DCO merger rates on the constraint-satisfying model parameters provides revised estimates for various phenomena of interest, such as for the BH-BH, BH-NS, and NS-NS merger rates. Figure 15 shows smoothed histograms of the BH-BH, BH-NS, and NS-NS merger rates, both before and after observational constraints were applied. Additionally, a smoothed curve shows the results modulated by the effect of systematic error. These results should be contrasted with the distinctly different post-constraint results shown in O'Shaughnessy et al. (2005b) (cf. their Figure 5 and C7). Notably, even though *two fewer* constraints were imposed, they find a significantly smaller (2% versus 9%) constraint-satisfying volume. In large part, these differences can be ascribed to including systematic errors: in O'Shaughnessy et al. (2005b), preliminary data for the sparse and poor-quality NSNS(vw) sample was fit and applied without any account for fit-induced errors. However, our calculation also differs at several fundamental levels from the original approach : (i) the space of models studied is larger, covering more area in v_1, v_2 (see,e.g., O'Shaughnessy et al. 2006a); (ii) the observed sample of merging NS-NS binaries is compared with the *total* merging NS-NS formation rate predicted from population synthesis, rather than with subset of merging NS-NS which undergo mass transfer; and critically (iii) the constraints are more numerous.

Finally, in Figure 16 we estimate the range of initial and advanced LIGO detection rates implied by these constrained results. This estimate combines our constrained population synthesis results; our estimates for systematic fitting error; the approximate LIGO range as a function of chirp mass M_c: $d = d_o \left(\mathcal{M}_c/1.2M_\odot\right)^{5/6}$ where $d_o = 15\sqrt{3/2}$, 300 Mpc for initial and advanced LIGO, respectively; estimates for the average volume detected for a given species, as represented by $\left\langle M_c^{15/6} \right\rangle = 111, 5.8, 2M_\odot^{15/6}$ for BH-BH, BH-NS, and NS-NS, respectively (see O'Shaughnessy et al. 2005b); and a homogeneous, Euclidean universe populated with Milky Way-equivalent galaxies with density $0.01\mathrm{Mpc}^{-3}$, each forming stars at rate $3.5M_\odot\mathrm{yr}^{-1}$. Updated rates that address a number of these simplifications will be examined in two forthcoming papers, O'Shaughnessy et al. (2006c) and O'Shaughnessy et al. (2006b).

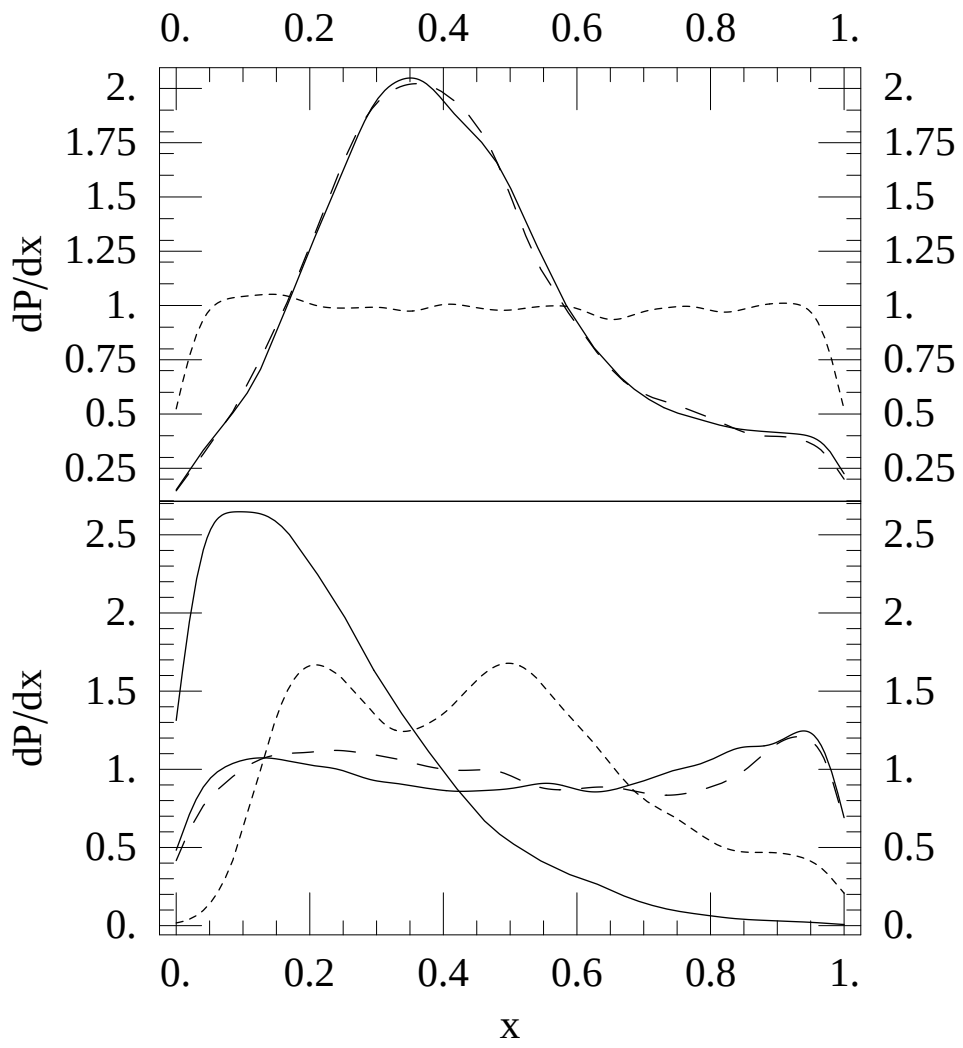

Fig. 14. Differential probability distributions dP_k/dx defined so $P_k(x)$ is the fraction of all models consistent with all DCO observations and with $x_k < X$. The top panel shows the distributions for the 3 kick-related parameters x_3, x_4, x_5 (dashed, solid, and dotted, respectively, corresponding to v_1, v_2, and s). The bottom panel shows the distributions for x_1 (the mass-ratio distribution parameter r, appearing as the solid nearly constant curve), and the three binary-evolution-related parameters x_2, x_6, x_7 (dashed, dotted, and solid, respectively, corresponding to w, $\alpha\lambda$, and f_a). The distribution of $f_a = x_7$ exhibits a strong peak somewhere between $0 - 0.1$; our choice of smoothing method causes all projected distributions to appear to drop to zero at the boundaries, as it involves averaging with empty cells.

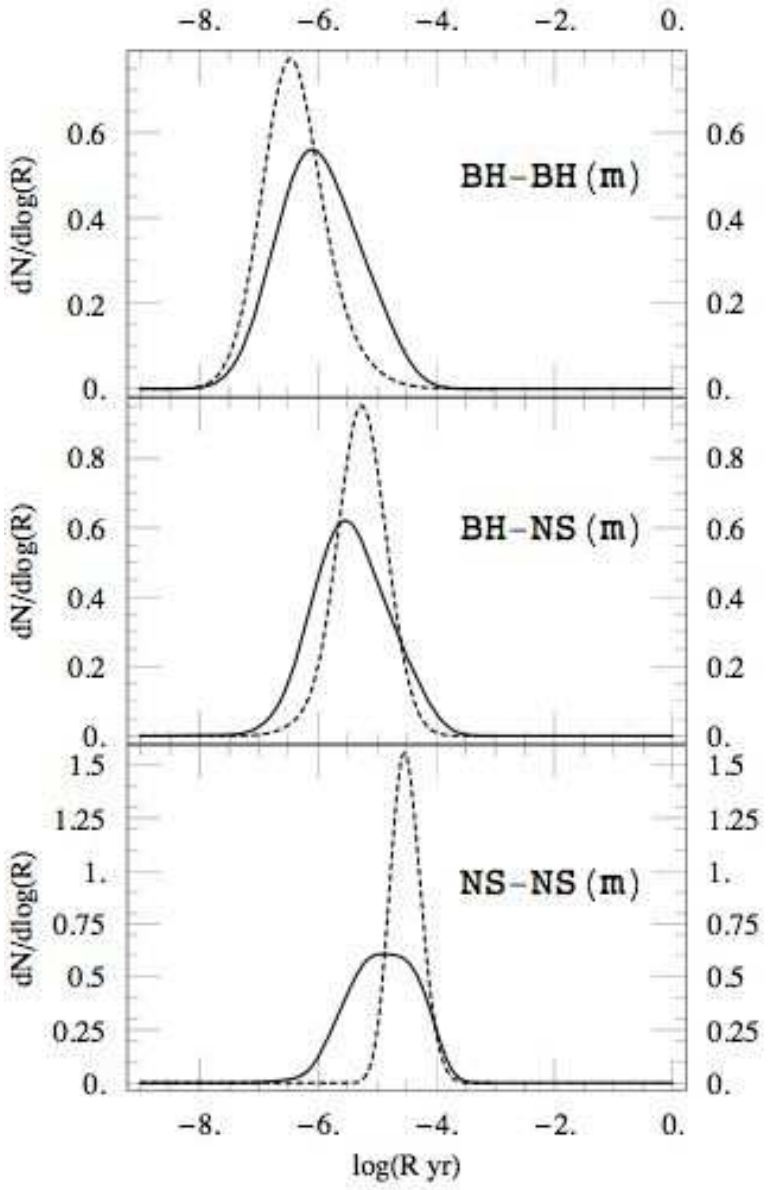

Fig. 15. A plot of the probability distributions for the BH-BH (top), BH-NS (center), and NS-NS (bottom) merger rates per Milky Way-equivalent galaxy, allowing for systematic errors in the BH-BH, BH-NS, and NS-NS fits. The solid curves result from smoothing a histogram of results from a random sample of population synthesis calculations with systematic errors included. The dashed curve shows the same results, assuming model parameters are restricted to those which satisfy all four DCO constraints (both WD-NS and both NS-NS constraints). Compare with Figure 5 of O'Shaughnessy et al. (2005b).

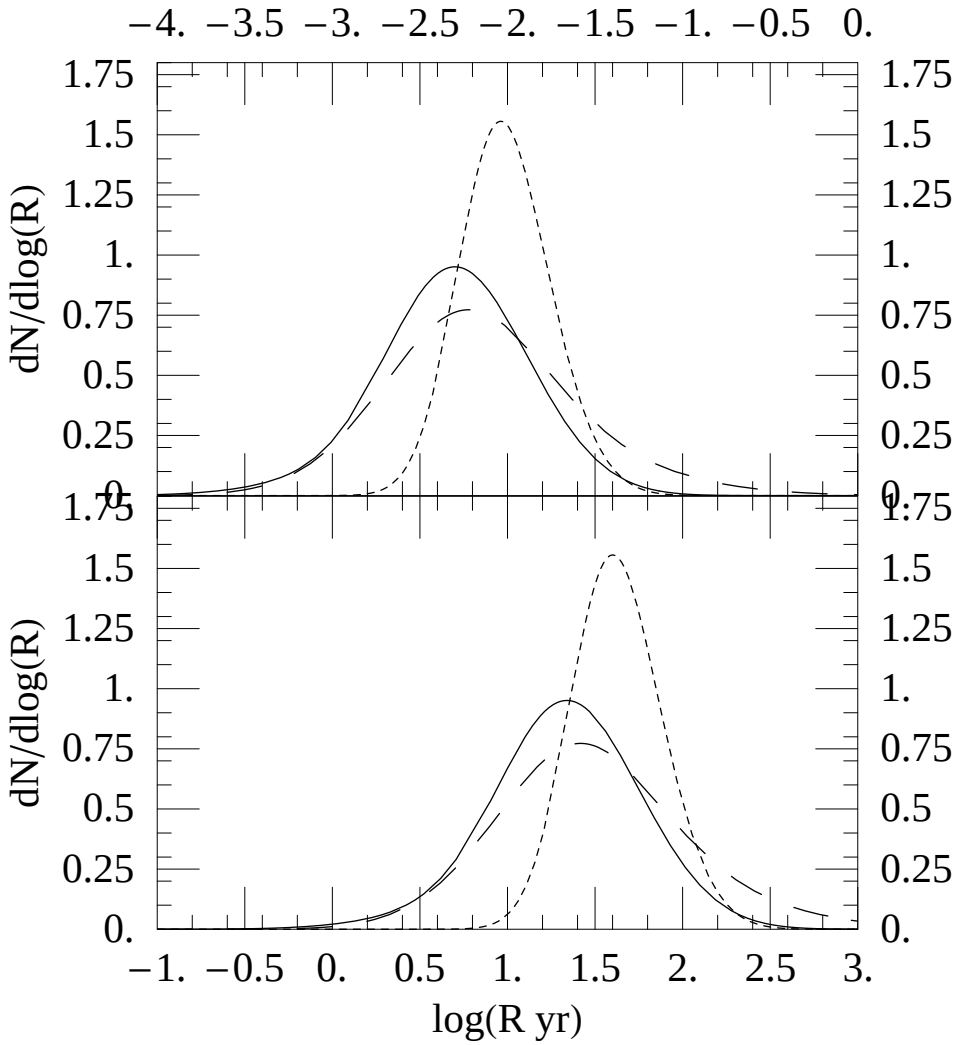

Fig. 16. Range of expected detection rates for initial (top) and advanced (bottom) LIGO for BH-BH (dashed), BH-NS (solid), and NS-NS (dotted) binaries, based on models that satisfy observational constraints and under the assumptions outlined in O'Shaughnessy et al. (2005b) (e.g., using a fixed chirp-mass spectrum and LIGO range for detection, as well as assuming Milky-Way like galaxies fill the universe with density $0.01\mathrm{Mpc}^{-3}$). These estimates incorporate systematic errors due to the fitting procedure.

5.7 Conclusions

O'Shaughnessy et al. (2005b) performed a proof-of-concept calculation to compare population synthesis simulations with observations, interpret the resulting constrained volume, and apply the constraint-satisfying parameters

to revise a priori predictions of astrophysically critical rate results. Here we demonstrate that even when systematic model fitting errors are aggressively overcompensated for, observational constraints still provide information about population synthesis parameters. These results include both surprisingly good agreement with pulsar kick distributions and strong constraints on at least one parameter involved in binary evolution. Since in almost all cases our systematic errors appear much smaller than those from observations, we are confident that now *observational* limitations, rather than computational ones, primarily limit our ability to constrain population synthesis results. In particular, we expect stringent tests of population synthesis models are possible, beginning by imposing more observational constraints than varied model parameters (seven in our case).

Our approach also strongly suggests that population synthesis estimates for DCO merger rates vary in a very complex manner, as indicated by the large χ^2 produced by even the best low-order polynomial fits to often often very high-quality data (see, e.g. O'Shaughnessy et al. 2006a). We strongly suspect that a more physically motivated class of basis functions could achieve a much better fit; we intend to explore this possibility, along with the reliability of purely nonparametric fits, in a future study.

Our analysis remains predicated upon a correct identification of all parameters and input physics critical for the formation of double compact objects. Admittedly, our understanding of binary evolution continues to evolve; however multiple population studies from different groups over the years lead to very similar conclusions about the basic input physics that primarily affects the formation rates of double compact objects (Belczynski et al. 2002b; Hurley et al. 2002; Portegies Zwart & Verbunt 1996; Fryer et al. 1998). In this paper we use a relatively new version of the *StarTrack* code that is described in great detail in Belczynski et al. (2006b). A forthcoming paper (Belczynski, Kalogera, & Bulik, in preparation) will discuss how these updates affect the evolutionary history and formation rates in significantly greater detail.

Our analysis also remains predicated upon a correct and complete interpretation of the observational sample and associated systematic and model uncertainties. In some respects, however, our models for observations and their biases may be incomplete or not representative. We effectively assume pulsar recycling is required to detect binary pulsars in our implicit hypothesis that only one pulsar in NS-NS systems, the one observed, was ever likely to have been detected. And finally we use a canonical value for pulsar beaming correction factor f_a for several systems with known spins but unknown beaming geometry. (We hope to address these questions in a forthcoming paper.)

Last, our analysis of DCO merger rates remains predicated on the assumption that the Milky Way formed stars at a relatively uniform rate for the last

10 Gyr. However, as will be demonstrated at greater length in two forthcoming papers (O'Shaughnessy et al. 2006b,c), if the star formation rate increased significantly when the Milky Way was young, then since most binaries would then form early in the lifetime of the Milky Way, the young-galaxy contribution could conceivably overwhelm the present-day contribution. In other words, the present-day Milky Way merger rate for BH-BH binaries, for example, could be completely determined by the star formation rate nearly 10 Gyr ago.

And to be comprehensive regarding the factors neglected here, our population synthesis parameter study has not varied over *all* plausible models. We have neither considered purely polar supernova kicks (see Johnston et al. 2005) nor changed the maximum NS mass from $2M_{\odot}$ nor even allowed for a heterogeneous birth population of single stars and binaries (a binary fraction of 100% is assumed in all models). And of course we continue to use a single fixed star formation rate for the Milky Way, rather than treat it as an independent uncertain but constrained parameter.

However, all these limitations can be remedied by closer study. Thus, we expect that either (i) all DCO merger rates will become determined to within $O(50\%)$ or better (based on the comparative accuracy to which we know NS-NS merger rates), or (ii) experimental data will conflict with the prevailing notion of binary population synthesis, revealing flaws and limitations in classical parametric models for binary stellar evolution.

6 Open Issues

It has now been more than 30 years since the discovery of the first binary pulsar that happened to also be the first binary with two neutron stars. This discovery has essentially led to the development of a whole sub-field in compact object astrophysics and progress in this area has also greatly contributed to the progress in the development of gravitational-wave observatories over these years.

As we anticipate the direct detection of gravitational waves from binary inspirals and the possible, associated discovery of black hole binaries, we also take advantage of pulsar timing observations to the fullest and continually try to improve our understanding of the origin of tight double compact objects. It is clear that a lot of progress has been particularly made in the last few years with the discovery of the highly relativistic, first double pulsar and additional double neutron stars, and the tremendous progress in proper motion and pulse profile evolution measurements. More interestingly, our standard way of thinking about double compact object formation is called to question with a number of intriguing suggestions and counter-suggestions put forward: do neutron stars

form through two different physical mechanisms depending on the mass of their immediate progenitor at the time of core collapse (Podsiadlowski et al. 2005; Piran & Shaviv 2005a; Willems et al. 2006; Stairs et al. 2006) do some or the majority of neutron stars receive minimal supernova kicks with magnitudes significantly smaller than $50\,\mathrm{km\,s^{-1}}$ (van den Heuvel 2004; Chaurasia and Bailes 2005; Ihm et al. 2006; Dewi et al. 2005). Furthermore, some of the older questions still persist: what is the basic physical mechanism for core collapse that also drives supernovae? Do most black holes form through fallback onto proto-neutron-stars and supernovae or through direct collapse? What is the mass function of black holes and how does it depend on metallicity? Why are neutron star masses so close to one another in double neutron stars? What really determines the birth spins and spin evolution of neutron stars and black holes?

Starting with the very basic question of the core collapse physical mechanism Hans Bethe was intrigued by many of these questions and naturally his interest evolved towards binary compact objects, their evolutionary history, and their potential as gravitational wave sources. Given the progress we have experienced since the discovery of the first DNS binary, it is reasonable to expect that with the combination of developments in pulsar searches and observations, of the rise of gravitational-wave detections and astrophysics, and of the progress in theoretical physical understanding and computational astrophysics we will be able to answer some of the basic remaining questions raised by the existence of binary compact objects in nature.

Acknowledgements The work summarized here has been supported by a wide range of research funding sources. VK is grateful for support from NSF Gravitational Physics grants No. PHYS-0121416 and PHY-0353111, a David and Lucile Packard Foundation Fellowship in Science and Engineering grant, and a Cottrell Scholar Award from the Research Corporation. K.B. acknowledges the support of KBN Grant No. 1P03D02228.

References

Abbott, B., et al. 2005, Phys. Rev. D, 72, 082002

Abramovici, A., et al. 1992, Science, 256, 325

Arzoumanian, Z., Cordes, J. M., & Wasserman, I. 1999, ApJ, 520, 696

Bailes, M., Ord, S. M., Knight, H. S., & Hotan, A. W. 2003, ApJ, 595, L49

Belczyński, K., & Kalogera, V. 2001, ApJ Letters, 550, L183

Belczynski, K., Bulik, T., & Kalogera, V. 2002, ApJ Letters, 571, L147

Belczynski, K., Kalogera, V., & Bulik, T. 2002, ApJ, 572, 407

Belczynski, K., Perna, R., Bulik, T., Kalogera, V., Ivanova, N., & Lamb, D. Q. 2006, ApJ, 648, 1110

Belczynski, K., Kalogera, V., Rasio, F. A., Taam, R. E., Zezas, A., Bulik, T., Maccarone, T. J., & Ivanova, N. 2006, ArXiv Astrophysics e-prints, arXiv:astro-ph/0511811

Bethe, H. A., & Brown, G. E. 1998, ApJ, 506, 780

Bethe, H. A., & Brown, G. E. 1999, ApJ, 517, 318

Bhattacharya, D., & van den Heuvel, E. P. J. 1991, Physics Reports, 203, 1

Brandt, N., & Podsiadlowski, P. 1995, Monthly Notices of the Royal Astronomical Society, 274, 461

Brown, G. E. 1995, ApJ, 440, 270

Burgay, M., et al. 2003, Nature, 426, 531

Camilo, F., Manchester, R. N., Gaensler, B. M., Lorimer, D. R., & Sarkissian, J. 2002, ApJ Letters, 567, L71

Camilo, F. 2003, in *Radio Pulsars* (ASP Conf. Ser.), eds. M. Bailes, D.J. Nice, & S.E. Thorsett (San Francisco), 302, 145

Cappellaro, E., Evans, R., & Turatto, M. 1999, A&A, 351, 459

Cappellaro, E., Riello, M., Altavilla, G., Botticella, M. T., Benetti, S., Clocchiatti, A., Danziger, J. I., Mazzali, P., Pastorello, A., Patat, F., Salvo, M., Turatto, M., & Valenti, S. 2005, A&A, 430, 83

Carlberg, R. G., & Innanen, K. A. 1987, Astronomical Journal, 94, 666

Champion, D. J., Lorimer, D. R., McLaughlin, M. A., Cordes, J. M., Arzoumanian, Z., Weisberg, J. M. & Taylor, J. H. 2004, MNRAS, 350, L61

Chatterjee, S., et al. 2005, ApJ Letters, 630, L61

Chaurasia, H. K., & Bailes, M. 2005, ApJ, 632, 1054

Chen, K. & Ruderman, M. 1993, ApJ, 402, 264

Chen, B., et al. 2001, ApJ, 553, 184

Coles, W. A., McLaughlin, M. A., Rickett, B. J., Lyne, A. G., & Bhat, N. D. R. 2005, ApJ, 623, 392

Cordes, J. M., Romani, R. W., & Lundgren, S. C. 1993, Nature, 362, 133

Cordes J.M. & Chernoff, D.F. 1997, ApJ, 482, 971

Cox, A. N. 2000, Allen's Astrophysical Quantities, 4th edn.

Demorest, P., Ramachandran, R., Backer, D.C., Ransom, S.M., Kaspi, V., Arons, J., & Spitkovsky, A. 2004, ApJ Letters, 615, L137

Dewi, J. D. M., Pols, O. R., Savonije, G. J., & van den Heuvel, E. P. J. 2002, Monthly Notices of the Royal Astronomical Society, 331, 1027

Dewi, J. D. M., & Pols, O. R. 2003, Monthly Notices of the Royal Astronomical Society, 344, 629
Dewi, J. D. M., & van den Heuvel, E. P. J. 2004, Monthly Notices of the Royal Astronomical Society, 349, 169
Dewi, J. D. M., Podsiadlowski, Ph., Pols, O. R. 2005, Monthly Notices of the Royal Astronomical Society, 363, L71
Dewi, J.D.M., Podsiadlowski, Ph., Sena, A. 2006, Monthly Notices of the Royal Astronomical Society, 368, 1742
Diehl, R., Halloin, H., Kretschmer, K., Lichti, G. G., Schönfelder, V., Strong, A. W., von Kienlin, A., Wang, W., Jean, P., Knödlseder, J., Roques, J.-P., Weidenspointner, G., Schanne, S., Hartmann, D. H., Winkler, C., & Wunderer, C. 2006, Nature, 439, 45
Edwards, R. T. & Bailes, M. 2001, ApJ Letters, 547, L37
Faucher-Giguere, C. -A., & Kaspi, V. M. 2006, ApJ, 643, 332
Faulkner, A. J., Kramer, M., Lyne, A. G., Manchester, R. N., McLaughlin, M. A., Stairs, I. H., Hobbs, G., Possenti, A., Lorimer, D. R., D'Amico, N., Camilo, F., & Burgay, M. 2005, ApJ Letters, 618, L119
Fryer, C., & Kalogera, V. 1997, ApJ, 489, 244
Fryer, C., Burrows, A., & Benz, W. 1998, ApJ, 496, 333
Habets, G. M. H. J. 1986, Astronomy & Astrophysics, 167, 61
Hills, J. G. 1983, ApJ, 267, 322
Hobbs, G., Lorimer, D. R., Lyne, A. G., & Kramer, M. 2005, Monthly Notices of the Royal Astronomical Society, 360, 974
Hulse R. & Taylor, J. H. 1975, ApJ, 195, L51
Hurley, J. R., Tout, C. A., & Pols, O. R. 2002, MNRAS, 329, 897
Ihm, C. M., Kalogera, V., & Belczynski, K. 2006, ApJ, in press [astro-ph/0508626]
Ivanova, N., Belczynski, K., Kalogera, V., Rasio, F. A., & Taam, R. E. 2003, ApJ, 592, 475
Jenet, F.A. & Ransom, S.M. 2004, Nature, 428, 919
Johnston, S., Hobbs, G., Vigeland, S., Kramer, M., Weisberg, J. M., & Lyne, A. G. 2005, MNRAS, 364, 1397
Junker, W., & Schäfer, G. 1992, Monthly Notices of the Royal Astronomical Society, 254, 146
Kalogera, V. 1996, ApJ, 471, 352
Kalogera, V., & Lorimer, D. R. 2000, ApJ, 530, 890
Kalogera, V. 2000, ApJ, 541, 319
Kalogera, V., Narayan, R., Spergel, D. N., & Taylor, J. H. 2001, ApJ, 556, 340
Kalogera, V., et al. 2004, ApJ Letters, 601, L179
Kalogera, V., et al. 2004, ApJ Letters, 614, L137
Kalogera, V., Kim, C., Lorimer, D. R., Ihm, M., & Belczynski, K. 2005, in ASP Conf. Ser. 328: Binary Radio Pulsars, ed. I. Stairs, 261
Kaspi, V. M., Lyne, A. G., Manchester, R. N., Crawford, F., Camilo, F., Bell, J. F., D'Amico, N., Stairs, I. H., McKay, N. P. F., Morris, D. J., & Possenti,

A. 2000, ApJ, 543, 321
Kim, C., Kalogera, V., & Lorimer, D. R. 2003, ApJ, 584, 985 (KKL)
Kim, C., Kalogera, V., Lorimer, D. R., & White, T. 2004, ApJ, 616, 1109
Kim, C., Kalogera, V., & Lorimer, D. R. 2006, in A life with stars [astro/ph/0608280]
Kramer, M. 1998, ApJ, 509, 856
Kramer, M., Lyne, A. G., Hobbs, G., Löhmer, O., Carr, P., Jordan, C., & Wolszczan, A. 2003, ApJ Letters, 593, L31
Kramer, M., et al. 2005, ArXiv Astrophysics e-prints, arXiv:astro-ph/0503386
Kramer, M., Stairs, I. H., Manchester, R. N., McLaughlin, M. A., Lyne, A. G., Ferdman, R. D., Burgay, M., Lorimer, D. R., Possenti, A., D'Amico, N., Sarkissian, J. M., Hobbs, G. B., Reynolds, J. E., Freire, P. C. C., & Camilo, F. 2006, Science, 314, 97
Kuijken, K., & Gilmore, G. 1989, Monthly Notices of the Royal Astronomical Society, 239, 571
Lorimer, D. R., et al. 2005, in *Binary Radio Pulsars* (ASP Conf. Ser.), eds. F. A. Rasio & I. H. Stairs (San Francisco), 328, 113
Lorimer, D. R., et al. 2006, ApJ, 640, 428
Lyne, A. G., Burgay, M., Kramer, M., Possenti, A., Manchester, R. N., Camilo, F., McLaughlin, M. A., Lorimer, D. R., D'Amico, N., Joshi, B. C., Reynolds, J., & Freire, P. C. C. 2004, Science, 303, 1153
Lyutikov, M. 2004, Monthly Notices of the Royal Astronomical Society, 353, 1095
Lyutikov, M., & Thompson, C. 2005, ApJ, 634, 1223
Manchester, R. N., et al. 2005, ApJ Letters, 621, L49
Narayan, R., Piran, T., & Shemi, A. 1991, ApJ Letters, 379, L17
Nomoto, K. 1984, ApJ, 277, 791
Nomoto, K. 1987, ApJ, 322, 206
O'Shaughnessy, R., Kalogera, V., & Belczynski, K. 2005, ApJ, 620, 385
O'Shaughnessy, R., Kim, C., Fragos, T., Kalogera, V., & Belczynski, K. 2005, ApJ, 633, 1076
O'Shaughnessy, R., Kalogera, V., & Belczynski 2006, submitted to ApJ [astro/ph/0609465]
O'Shaughnessy, R., Kalogera, V., & Belcynski, K. 2006, in preparation
O'Shaughnessy, R., Belczynski, C., Kalogera, V., & Lamb, D. 2006, in preparation
Paczynski, B. 1990, ApJ, 348, 485
Peters P. C. & Mathews, J. 1963, Phys. Rev. D, 131, 435
Pfahl, E., Rappaport, S., Podsiadlowski, P., & Spruit, H. 2002, ApJ, 574, 364
Phinney, E. S. 1991, ApJ, 380, L17
Piran, T., & Shaviv, N. J. 2005, Physical Review Letters, 94, 051102
Piran, T., & Shaviv, N. J. 2005, ArXiv Astrophysics e-prints, arXiv:astro-ph/0510584
Piran, T., & Shaviv, N. J. 2006, ArXiv Astrophysics e-prints, arXiv:astro-ph/0603649

Pinsonneault, M.H. & Stanek, K.Z. 2006, ApJ, 639, L67
Podsiadlowski, P., Dewi, J. D. M., Lesaffre, P., Miller, J. C., Newton, W. G., & Stone, J. R. 2005, Monthly Notices of the Royal Astronomical Society, 361, 1243
Portegies Zwart, S. F. & Verbunt, F. 1996, A&A, 309, 179
Portegies Zwart, S. F. & Yungelson, L. R. 1998, A&A , 332, 173
Ransom, S. M., Kaspi, V. M., Ramachandran, R., Demorest, P., Backer, D. C., Pfahl, E. D., Ghigo, F. D., & Kaplan, D. L. 2004, ApJ Letters, 609, L71
Stairs, I. H., Thorsett, S. E., & Arzoumanian, Z. 2004, Phys. Rev. Lett., 93, 141101
Stairs, I. H., Thorsett, S. E., Dewey, R. J., Kramer, M., & McPhee, C. A. 2006, MNRAS, in press [astro-ph/0609416]
Stokes, G. H., Taylor, J. H., & Dewey, R. J. 1985, ApJ, 294, L21
Tauris, T. M., & van den Heuvel, E. 2006, ArXiv Astrophysics e-prints, arXiv:astro-ph/0303456
Thorsett, S. E., Dewey, R. J., & Stairs, I. H. 2005, ApJ, 619, 1036
van den Bergh, S. & Tammann, G. A. 1991, ARA&A, 29, 363
van den Heuvel, E. P. J. 2004, Proceedings of 5th INTEGRAL Workshop on the INTEGRAL Universe, 185
van Kerkwijk, M. H. & Kulkarni, S. R. 1999, ApJ, 516, L25
Weisberg, J. & Taylor, J. H. 2002, ApJ, 576, 942
Wex, N., Kalogera, V., & Kramer, M. 2000, ApJ, 528, 401
Willems, B., & Kalogera, V. 2004, ApJ Letters, 603, L101
Willems, B., Kalogera, V., & Henninger, M. 2004, ApJ, 616, 414
Willems, B., Henninger, M., Levin, T., Ivanova, N., Kalogera, V., McGhee, K., Timmes, F. X., & Fryer, C. L. 2005, ApJ, 625, 324
Willems, B., Kaplan, J., Fragos, T., & Kalogera, V. 2006, Phys. Rev. D, 74, 043003
Wolszczan, A. 1991, Nature, 350, 688
Zou, W. Z., Hobbs, G., Wang, N., Manchester, R. N., Wu, X. J., & Wang, H. X. 2005, Monthly Notices of the Royal Astronomical Society, 362, 1189